Mean-Square Resonator

And Relation to the Duffing Resonator

Shane Rupert Koscielniak

TRIUMF Beam Note: TRI-BN-24-36

Contents

Chapter 1

Mean-Square Oscillator

1.1 Introduction

This article has three main themes: (1) the properties of an oscillator with restoring force $(\alpha + \beta\langle x^2\rangle)x$ where $x(t)$ is the oscillation and $\langle \dots \rangle$ denotes the time average over one or more oscillations; (2) triple-valued frequency response; and (3) a direct explanation of the jumps between the largest and smallest values. The oscillator with force law $(\alpha + \beta\langle x^2\rangle)x$ has been encountered in the context of radio-frequency cavity resonators since 1967[1] but is un-named; we call it the mean-square oscillator (MSO).

The anharmonic oscillator with cubic non-linearity (or Duffing oscillator) has the restoring force $(\alpha+\beta x^2)x$ where $x(t)$ is the oscillation. A resonator is a driven oscillator. The oscillation frequency[1] of the Duffing oscillator (DO) depends on the amplitude. The steady state response of the Duffing[2] resonator as a function of excitation frequency and excitation amplitude is well known: at small amplitude the response is single-valued at all frequencies, whereas (above a threshold amplitude) it becomes triple-valued in a range of frequency around the resonance. Further, if the excitation frequency is swept, the behaviour differs dramatically between upward and downward sweeps. At two specific frequencies, the response jumps up, or jumps down, between the smallest and largest values of the steady state response. Given that it is simple to derive the steady state (SS) response, it comes as a surprise that the oscillator displays these dramatic behaviours. Although the internal feedback mechanism responsible is easy to describe, explanatory accounts[5, 6, 10, 11, 12] are usually sophisticated, complicated and approximative. Typically the explanation comes as a *post mortem*, but a prenatal assessment that provides a direct explanation would be preferable.

Remarkably, the crucial question "how did the oscillator come to be in the steady state?" is rarely asked. How did the oscillation amplitude progress from zero to a large value? The steady state solution is an infinite-time solution: it persisted so in the deep past, and will continue so into the deep future so long as the drive is not removed. Evidently, it is a mathematical artifact. In reality, the system had to be prepared in some way. For the linear oscillator, there are mathematical tools to describe two modes of preparation. The effect of turning on a fixed frequency drive at time $t = 0$ and the ensuing amplitude growth is calculated by the method of Green's functions. The effect of slowly sweeping the excitation frequency through the resonance is computed by the Fresnel integrals. [The response maximum is shifted in the direction of the sweep and is smaller than the steady state value, because there is insufficient time for the amplitude to build up before the excitation moves to a different frequency; and there are subsidiary maxima due to interference between the responses at different frequencies. These effects become insignificant when the slew rate is very much less than the damping rate.] Unfortunately, these methods cannot be applied to nonlinear oscillators.

[1] To be precise, the fundamental Fourier component; because free oscillation of the DO has an infinite set of harmonics.

The same equation of motion that describes preparation of the steady state also generates the jumps. Given that we are interested in the oscillator response as a function of frequency, we shall explore the consequences of preparing the system by swept frequency starting at values very distant from the resonance frequency. It may be thought that if the sweep is extremely slow, the response will *at all times* be a state extremely close to equilibrium. (This is an assumption built into the simple derivation of the steady state values.) However, because of the internal feedback mechanism (βx^2) due to the oscillator non-linearity, there are two characteristic frequencies (the jump values) at which the system diverges into violent disequilibrium; and it does so even for infinitesimal slew rate of the drive frequency.

Going forward we shall prototype the behaviour of the Duffing resonator by that of a simpler resonator having restoring force $(\alpha+\beta\langle x^2\rangle)x$. Unlike the DO, the MSO does not generate harmonics and sub-harmonics of the drive frequency, and is therefore mathematically simpler. We adopt standard methods from the DO analysis to the mean-square oscillator; and results from the MSO analysis carry back to the DO.

1.1.1 Article structure

Sections 1.1.2,1.1.4 define the relevant physical and mathematical quantities. Sec. 1.1.3 references standard texts on the DO, and a thumbnail sketch of recent numerical work on DO bistability. Sec. 1.2 introduces the steady state and dynamic equilibrium state of the MSO, and also terminology relating to properties of the resonance curve. Secs. 1.2.7 and 1.2.8 demonstrates two tools that are later used in the linear (Sec. 1.3) and nonlinear (Sec. 1.4) instability analyses. Sec. 1.5 explains that the jump dynamics is essentially the poles of the derivative dR/dw. Sec. 1.6 presents numerical examples of frequency sweeps and jump phenomena. Sec. 1.7 explains the generic origin of the MSO; while Sec. 1.7.1 presents two concrete examples. Sec. 1.8 summarises the present work and makes the case that it applies also to the Duffing Oscillator. Sec. A presents additional examples that augment those in the main text. Sec. B offers a commentary on the existence and uniqueness proofs of Urabe. Sec. C provides an account of the multiple-scales explanation of bistability and the jumps.

1.1.2 List of symbols

- $\langle x^2\rangle$ mean square value.
- $F(x) = \alpha x + \beta\langle x^2\rangle x$ is restoring force.
- α and β are linear and cubic force constants, respectively.
- $\sqrt{\alpha}$ angular resonance frequency when $\beta = 0$ and $\delta = 0$.
- δ damping rate.
- $\epsilon = \delta/\sqrt{\alpha}$ normalized damping rate.
- ω drive angular frequency.
- $w = \omega/\sqrt{\alpha}$ normalized drive frequency.
- $\sigma = \dot{\omega}/\alpha$ normalized sweep rate or frequency slew.
- γ drive amplitude.
- $\rho = \beta\gamma^2/\alpha^3$ dimensionless variable that characterises degree of nonlinearity.
- $\chi = 2\rho/\epsilon^2$ dimensionless variable that characterises effect of damping on nonlinearity.
- $\lambda = w^2 - 1$ renormalized "frequency" scale.
- R amplitude response; R^2 power response.
- $R_\rho = R^2\rho$ renormalized power response.

- A, B the in-phase and quadrature components, respectively, of R.
- $\lambda_r, \hat{R}_\rho$ frequency and power at the maximum of the resonance curve $dR_\rho/d\lambda = 0$.
- $(\lambda_l, R_{\rho\,l})$ lower turning point $d\lambda/dR_\rho = 0$ and distant from $(\lambda_r, \hat{R}_\rho)$.
- $(\lambda_u, R_{\rho\,u})$ upper turning point $d\lambda/dR_\rho = 0$ and close to $(\lambda_r, \hat{R}_\rho)$.
- Where $|\lambda_u| \geq |\lambda_r|$ and $|R_{\rho\,u}| \leq |\hat{R}_\rho|$; where $|\lambda_u| \geq |\lambda_l|$ and $|R_{\rho\,u}| \geq |R_{\rho\,l}|$.
- The lower/upper turning point is the location of the jump up/down.
- $(\lambda_s, R_{\rho\,s})$ location of linear-instability threshold on the upper branch.
- $(\lambda_t, R_{\rho\,t})$ location of linear-instability threshold on the lower branch.
- When R_ρ is single valued, $|\lambda_r| < |\lambda_s| < |\lambda_t|$.
- When R_ρ is multi-valued, $|\lambda_r| < |\lambda_s| < |\lambda_u|$ and $|\lambda_l| < |\lambda_t| < |\lambda_u|$.

1.1.3 Duffing resonator literature

The anharmonic oscillator with linear and cubic terms was studied by A.M. Legendre, N.H. Abel and C.G.J. Jacobi circa 1800. The Duffing[2] resonator was introduced in 1918 and has a vast and growing literature; most of it post 1970. Chapter 5.4.3 of Magnus' book[3] contains a brief and approximative introduction to the Duffing Resonator (DR). Chapter 1 of Hagedorn's book[6] contains many results relating to the DR, and gives an explanation of the jumps. The book[7] of Kovacic and Brennan, and contributors, presents a survey of the field circa 2011, collects together many of the known results, and has extensive references. One infelicity of Ref.[7] is that some of the contributions and expressions are careless with respect to the small quantity ϵ^2; replacing $(1-\epsilon^2/4)$ by 1 eradicates the distinction between turning points and linear-instability thresholds.

Article 3 by Yabuno[8] explores free oscillations in terms of the location and properties of the fixed points when there is no drive. Article 4 by Cveticanin[9] presents a variety of mathematical techniques uses to analyze the DR behaviour. Article 5 by Kalmar-Nagy[10] presents a summary of the steady state conditions, and linear stability analysis. Article 6 by Mallik[11] presents additional analyses: the method of fast/slow variables (also called multiple-scales) is used to explain the jump phenomena near the primary resonance $w = 1$; and the Mathieu equation is employed to map the stability domain at the secondary resonances $w = 3, \frac{1}{3}$. Both articles 5 & 6 discuss properties of the maximum and turning points of the resonance curve; and both drop terms in ϵ^2. Use of "cusp catastrophe" to explain the jump is referenced, but not presented.

None of these texts above pay attention as to how the steady state of the resonator is prepared. In 2021, Wawrzynski[13] attempted to address that issue. In addition to the customary slow frequency sweeps $\omega(t)$ at fixed excitation amplitude, he widens the concept of bistability to include slow increase of excitation amplitude $\gamma(t)$ at fixed frequency, and the use of small impulses to initiate transitions (jumps). Using Eq. 1.3 with $\beta\langle x^2\rangle x$ replaced by βx^3, the equation of motion is solved by numerical methods, and the outcomes (stable or jumps, etc.) are used create a "chart of bistability" areas in the plane of $R(\omega)$. He eschews the dimensionless variable ρ used in Eq. 1.4 because he is incredulous that ρ is a sufficient metric for nonlinearity; and so takes a sparse grid of parameters $\alpha, \beta, \delta, \gamma$. We disagree: the system is consistent with the Buckingham[2] Π-theorem; there are 4 variables and 2 dimensionless groups ρ and χ. Based on limited data[3] he subdivides the DR response $R(\omega)$ into several areas[4] based on their qualitatively different behavior. This broader definition of bistability is compared against the limited and approximate theoretical results in Brennan[15], and the latter found to be inadequate. Given the variety of system preparation,

[2] If there are n variables in a problem and these variables contain m primary dimensions the equation relating all the variables will have $(n - m)$ dimensionless groups.

[3] 3 values of α, 3 values of $\beta < 0$, 8 values of δ and 2 values of γ; the drive ω is scanned.

[4] It would be better to call them *regions*, but Wawrzynski reseves the term "region" for a frequency range.

and the limitations in Ref.[15], the conclusion is not unexpected. In 2022 Wawrzynski[14] uses numerical curve fitting to find analytic formulae that delineate (enclose or define) different regions in his bistability chart. In particular, he wishes to find the "origin point", that is the parameter values at which bistability emerges. He appears unaware of Ref. [11] Sec. 6.4.1. which derives the origin point. It is clear that Wawrzynski recognizes that "system preparation" is an important aspect of the nonlinear system; has widened the range of parameters affecting jump conditions; and has found some new and interesting effects. However, the analysis is weak and the generality compromised by the refusal to use dimensionless parameters.

Existence and uniqueness

It is not self-evident that a sinusoidal-driven arbitrary nonlinear oscillator has a periodic steady state; and to assume so would be an act of faith. It is not even obvious that the response of the MSO or DSO to a sinusoid is sinusoidal. These issues are not addressed in Ref. [7]. For the DO, which generates an infinite set of harmonics, the periodic state may seem implausible and/or artificial - and hints at chaotic motion. Nevertheless, there is a body of literature (e.g. Groves[16]) which attempts to determine, by purely analytic means, consistency conditions for large numbers of harmonics. Clearly, *existence and uniqueness theorems* are needed.

For a wide class of periodically-driven nonlinear second-order differential equations Hale[17] (in 1963) and independently Urabe[18] (in 1965) have established an existence theorem and proven the uniqueness of periodic solutions (Fourier series). It is not entirely clear if these (similar) proofs extend to the strong nonlinear case. Hagedorn's book[6] presents another existence proof based on Brouwer's theorem[5] for the fixed points of mappings between abstract spaces.

Hale and Urabe substitute a trial combination of harmonics into the driven ODE, leaving a residual. One at a time, the residual is multiplied by each of the Fourier basis functions and integrated over the period of the fundamental; and the result set equal to zero. This gives a system of (nonlinear) algebraic equations (SNAE) for the Fourier coefficients which are solved by Newton iteration, leading to a convergence criterion. Urabe's proofs stipulates: (i) that the equation of motion and its derivatives with respect to time t and the solution x be both continuously (infinitely) differentiable; (ii) the derivatives be bounded (i.e. finite); (iii) that the Jacobian determinant be invertible. And there is the additional caveat, for uniqueness: the number of terms in the Fourier series must must be sufficiently large. Urabe[19] also furnishes a numerical scheme, based on Newton iteration, for finding the Fourier coefficients and proves the iterants converge. Urabe[20] proves also that the method is superior to schemes which average over high-frequency components. Urabe consistently calls his manipulation of Fourier harmonics the Galerkin method; and this is explained in Appendix B.

1.1.4 Dimensionless variables

The four parameters $[\alpha, \beta, \delta, \gamma]$ are defined by their use in Eq. 1.3. If $x(t)$ is dimensionless, the parameters have the corresponding dimensions [Hz^2, Hz^2, Hz, Hz^2]. The response, as function of frequency, is obtained from the solution of Eq. 1.3. The expression, and the properties derived from it, has many terms, and is complicated. In the interest of simplification, we shall introduce dimensionless parameters. The loss of direct connection to $\alpha, \beta, \delta, \gamma$ is more than compensated by the brevity of the results. Moreover, the number of parameters is reduced from four to two. We introduce the linear transformations $t \to z/\sqrt{\alpha}$ and $x(z) \to (\gamma/\alpha)y(z)$; followed by $\omega \to w\sqrt{\alpha}$ and $\delta \to \epsilon\sqrt{\alpha}$ and $\beta \to \rho\alpha^3/\gamma^2$. Thus w and ϵ are normalized drive frequency and damping rate, respectively. The control parameter ρ makes clear that β alone does not determine the degree

[5] Brouwer's is a fixed-point theorem in topology, named after Dutch mathematician and philosopher L. E. J. (Bertus) Brouwer (1881-1966). Fixed point theorems are examples of existence theorems, in the sense that they assert the existence of objects, such as solutions to functional equations, but not necessarily methods for finding them.

of non-linearity; for any finite value of β we may find an excitation amplitude γ that makes the non-linearity strong. What may become lost under these transformations, is that when $\rho = 0$ the system reverts to a simple harmonic oscillator, in $y(z)$, with unit drive; as may be found by inspection of Eq. 1.4. Euler[21] discovered the resonant behaviour of the SHO; for given α the frequency response is a single parameter (δ) family of curves. In contrast, the DO and MSO for given α, β have a two-parameter (δ, γ) family of frequency response curves. This is fortuitous, because it allows to locate the resonance at small excitation γ before exploring the behaviour at large γ.

In an engineering or experimental context, it is customary to initially probe the resonance with small excitation (known as "signal level") before driving to large amplitudes. The condition for *signal level* is $|\beta|x^3 \ll \alpha x$. If the system were linear, then the maximum value would be $x^2 = \gamma^2/(\alpha\delta^2)$ as occurs at resonance. Combining these conditions we find $|\beta|\gamma^2/(\alpha\delta)^2 \ll 1$. We rewrite this in terms of the dimensionless parameters: signal level means $|\rho|/\epsilon^2 \ll 1$; and much less means a factor of 100 times smaller than unity. Thus $|\rho|/\epsilon^2 \simeq 1$ corresponds to very strong drive.

The quantity x^2/γ^2 is the power amplification, and $|x/\gamma|$ the amplitude magnification factor. We need to identify these quantities when written in terms of other quantities:

$$\frac{x^2}{\gamma^2} = \frac{y^2}{\alpha^2} \equiv \frac{R^2}{\alpha^2} \tag{1.1}$$

where $R(\epsilon, \rho, w)$ is the steady state amplitude. The actual power level is, of course, simply proportional to x^2; which may be written

$$x^2 = \left(\frac{y^2}{\alpha^2}\right)\gamma^2 \equiv \frac{R_\rho}{\rho}\frac{\gamma^2}{\alpha^2} = \frac{\alpha}{\beta}R_\rho(\epsilon, \rho, w) \quad \text{where} \quad \rho = \frac{\beta\,\gamma^2}{\alpha^3} \tag{1.2}$$

and where $R_\rho \equiv R^2 \times \rho$ is introduced below. Eq. 1.2, at fixed α, β, allows to map out the power response as a function of excitation amplitude γ or equivalent ρ as shown in Fig. 1.1. The shape of the resonance curve is created by the competition between drive and dissipation. In particular, dissipation limits the resonance maximum.

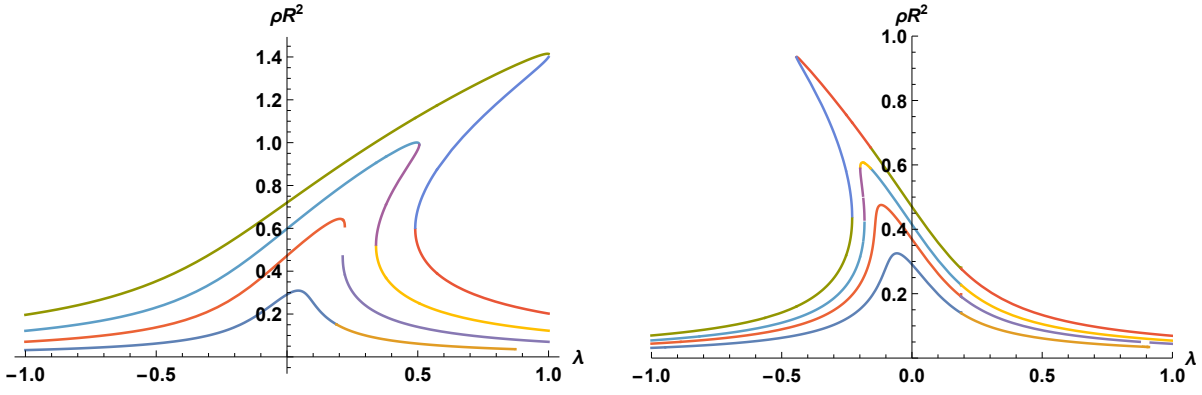

Figure 1.1: Resonator response R_ρ versus drive "frequency" λ. In every case $\epsilon = 0.1$ Left: hardening resonator, with increasing $+\rho = [0.001, 0.005, 0.015, 0.04]$ from bottom to top. Right: softening resonator, with increasing $-\rho = [0.001, 0.002, 0.003, 0.0049]$. The colour codes denote the cubic solutions x_1, x_2, x_3.

1.2 MSO Driven Response

Let t, x and $p = \dot{x}$ be time, position and momentum; and dots denote time derivatives ($dx/dt \equiv \dot{x}$). Consider the driven oscillator:

$$\ddot{x} + \dot{x}\delta + x\alpha + \langle x^2\rangle\beta x \;=\; \gamma\cos\phi(t)\;. \tag{1.3}$$

In the limit $\delta \to 0$ and $|x| \to 0$ and $\gamma = 0$, the resonance angular frequency is $\omega_{\rm res} = \sqrt{\alpha}$. In the case of fixed frequency excitation, $\phi = \omega t$ where ω is the drive frequency. For swept frequency excitation, $\omega(t) = \omega_0 + \dot{\omega}t$ with slew rate $\dot{\omega}$, the phase is $\phi(t) = \int_0^t \omega(u)du = \omega_0 t + \frac{1}{2}\dot{\omega}t^2$.

Under the transformations the phase becomes $\phi(z) = wz$ for fixed frequency, and $\phi = w_0 z + \frac{1}{2}\sigma z^2$ for swept frequency; where $w_0 = \omega_0/\sqrt{\alpha}$ and $\sigma = \dot{\omega}/\alpha$. Let primes denotes derivatives with respect to z; for example $A' \equiv dA/dz$. The equation of motion (EOM) becomes:

$$y'' \,+\, \epsilon y' \,+\, y \,+\, \langle y^2\rangle\rho\, y \;=\; \cos\phi(z)\;. \tag{1.4}$$

It is standard to take the trial solution $y(z) = [A(z)\cos\phi + B(z)\sin\phi]$. The assumption of phase synchronism between drive and response may seem artificial; but there is a phase variation implicit in the ratio B/A. Substitution of the trial in the EOM yields:

$$C_1\cos\phi + S_1\sin\phi \,+(\epsilon\cos\phi - 2w\sin\phi)A' \,+(2w\cos\phi + \epsilon\sin\phi)B' + A''\cos\phi + B''\sin\phi \;=\cos\phi\,. \tag{1.5}$$

$$\text{where}\quad C_1 = A + \rho A R^2/2 + (\sigma+\epsilon w)B - Aw^2 \quad\text{and}\quad S_1 = B + \rho B R^2/2 - (\sigma+\epsilon w)A - Bw^2 \tag{1.6}$$

and $R^2 \equiv (A^2 + B^2)$. Assuming that the system is in equilibrium implies that the derivatives A', B', A'', B'' are all zero. The simultaneous equations $C_1 = 1$ and $S_1 = 0$ may be solved for A, B:

$$A = R^2(2 + R^2\rho - 2w^2)/2 \quad\text{ and }\quad B = (\sigma + \epsilon\, w)R^2\;. \tag{1.7}$$

Comparison of the D.C. components $\langle(\cos\phi)^2\rangle = \langle y^2\rangle = (C_1^2 + S_1^2)/2$ yields the condition

$$R^2[4(\sigma + \epsilon\, w)^2 + (2 + R^2\rho - 2w^2)^2] \;=\; 1\;. \tag{1.8}$$

We may draw two conclusions from Eqs. 1.7 and 1.8. First, that under the condition of a uniform sweep of the drive frequency, there is a dynamic equilibrium state. Second, that provided $|\sigma| \ll \epsilon\, w$ the dynamic equilibria differ little from the steady state at fixed drive frequency. The case of fixed-frequency excitation is recovered by setting $\sigma = 0$.

The ratio of A/B implies a phase shift ψ compared with the drive sinusoid. Writing $A\cos\phi + B\sin\phi = R\cos(\phi + \psi)$, we find

$$\tan\psi = -\frac{B}{A} \;=\; \frac{-(\sigma + \epsilon\, w)}{(1 - w^2) + R_\rho/2}\;. \tag{1.9}$$

where $R_\rho = R^2\rho$ and R^2 is a root of Eq. 1.8; or equivalent $R_\rho(w)$ is a root of Eq. 1.11.

Equation 1.8 is a cubic equation. Nevertheless, provided that the quantity $R_\rho \equiv R^2\rho$ is sufficiently small, the response is

$$R^2 \approx \frac{1}{(\sigma + \epsilon\, w)^2 + (1 - w^2 + R_\rho/2)^2} \quad\begin{matrix}\text{compared}\\ \text{with}\end{matrix}\quad R^2(\sigma = 0, R_\rho = 0) = \frac{1}{(\epsilon\, w)^2 + (1 - w^2)^2}\,. \tag{1.10}$$

The appropriate regime is $R_\rho \ll 1$; and this occurs in two cases. When $\rho = 0$, the maximum is $R^2 = 1/\epsilon^2$. Thus when $|\rho|/\epsilon^2 \ll 1$ the approximation is valid across the resonance. In this case, the effect of the non-linearity is to broaden and shift the resonance. The second case is the small-amplitude tails far from resonance, where $|R_\rho| \ll 1$ always holds.

Equation 1.8 is a cubic equation for R^2. The roots of this equation are the equilibrium amplitudes-squared. There is a general expression for the roots of a cubic; and it will contain

terms like $\sqrt{\rho^6} = \pm\rho^3$ which are the cause of ambiguity - given that ρ itself may be positive or negative. This is avoided when we introduce the scaled variable $R_\rho = R^2 \times \rho$. The corresponding cubic equation is

$$R_\rho^3 + 4(1-w^2)R_\rho^2 + 4[(1-w^2)^2 + (\sigma + \epsilon\, w)^2]R_\rho - 4\rho = 0\,. \tag{1.11}$$

To make expressions more compact, we make one final change of variable: $\lambda \equiv w^2 - 1 = (\omega^2/\alpha) - 1$. In the limit $\gamma \to 0$, the resonance is centred at $\lambda = 0$. We may rewrite the phase shift in simpler form: $\tan\psi = \epsilon\sqrt{1+\lambda}/(\lambda - R_\rho/2)$. In the following, we shall explore the roots R_ρ of

$$R_\rho^3 \; - 4\lambda R_\rho^2 \; + 4[\lambda^2 + (\sigma + \epsilon\, w)^2]R_\rho \; - 4\rho = 0\,, \tag{1.12}$$

as a function of the scaled drive frequency λ and the two control parameters ϵ and ρ. In practice, $|\sigma| \ll \epsilon$ and $w \simeq 1$; and so the value of the shift in the roots induced by σ is almost insignificant. But, nevertheless, it introduces hysteresis. Going forward, we shall set $\sigma = 0$ unless otherwise stated. Hence the coefficient of R_ρ becomes $4[\lambda^2 + \epsilon^2(1+\lambda)]$. For small values of $|\rho|$, there is a single real root over the entire range of λ. Above a threshold value of $|\rho|$, there is a range of λ for which there are three real roots; the limits of this range are the jump frequencies; outside this range, there is a single real root.

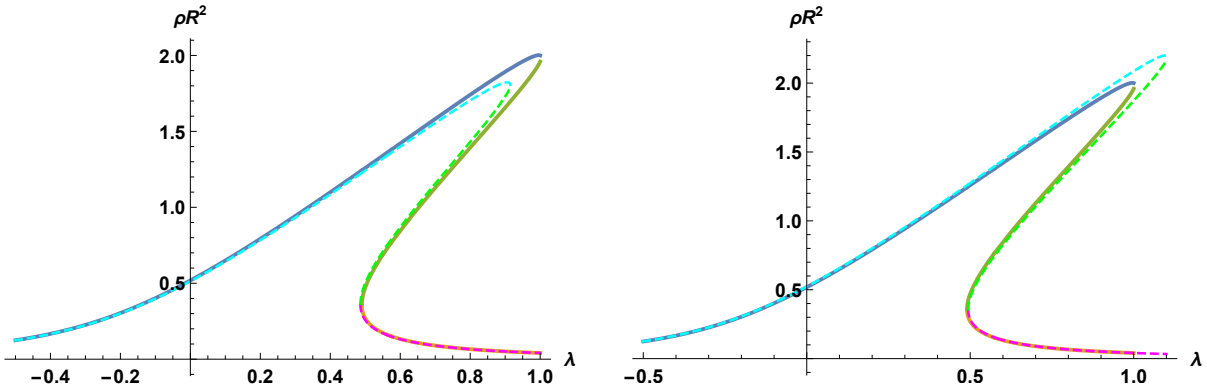

Figure 1.2: Superposed resonance curves for $(\epsilon = 0.1, \rho = 0.04)$ and $\sigma = 0$ or $|\sigma| = 0.01$. The case $\sigma \neq 0$ is given by the cyan, magenta and green dashed segments; the colours map to the solutions x_1, x_2, x_3 respectively. The case $\sigma = 0$ is given by the gun-blue, gold and olive-green solid segments. Left: sweep up. Right: sweep down.

1.2.1 Comparison of steady state and dynamic equilibrium

The steady-state solutions Eqs. 1.7, 1.8 are also known as the fixed points of Eqs. 1.5, 1.6. We compare graphically the equilibrium solutions when $\sigma \neq 0$, the dynamic equilibrium, and when $\sigma = 0$ the true steady state. For the examples, we have taken σ unrealistically large; about a factor one hundred larger than would be used in practice. This exaggeration is used to make the differences between the solutions clearly visible. The two examples here are up-sweeps and down-sweeps for the hardening resonator Fig. 1.2 and softening resonator Fig. 1.3. Although the differences are pronounced in the vicinity of resonance, they persist across the entire frequency range as shown in Figs. A.1 and A.2

We must be cautious about using the terms "sweep-up" when $\sigma > 0$ and "sweep-down" when $\sigma < 0$, because the hypothetical resonance curves are triple-valued. Even if the middle branch were stable, the curve cannot be produced by monotonic variation of the drive; the frequency would have to dither up/down. No middle branch occurs when a monotonic frequency sweep experiment is

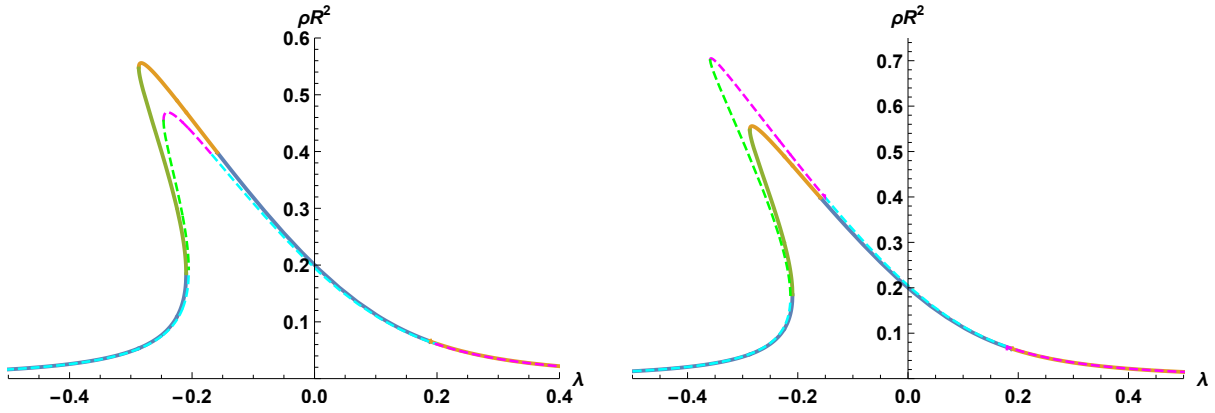

Figure 1.3: Superposed resonance curves for $(\epsilon = 0.1, \rho = -0.004)$ and $\sigma = 0$ or $|\sigma| = 0.005$. The case $\sigma \neq 0$ is given by the cyan, magenta and green dashed segments. The case $\sigma = 0$ is given by the gun-blue, gold and olive-green solid segments. Left: sweep up. Right: sweep down.

performed. A final comment: although Eqns. 1.7, & 1.8 are an improvement over their counterparts with $\sigma \equiv 0$, nevertheless they are not true to the real dynamics because the terms $\dot{A}, \ddot{A}$ and $\dot{B}, \ddot{B}$ have been set to zero.

1.2.2 Roots of cubic equations

The cubic equation has either three real roots, or one real root and two complex roots. From this stems the single- or triple-valued nature of the steady state amplitude. The general cubic equation $a_0 + a_1 x + a_2 x^2 + x^3$ has the formal solutions

$$x_1 = -\frac{a_2}{3} - \frac{2^{1/3}(3a_1 - a_2^2)}{3Z^{1/3}} + \frac{Z^{1/3}}{3 \times 2^{1/3}} \tag{1.13}$$

$$x_2 = -\frac{a_2}{3} + \frac{(1 + i\sqrt{3})(3a_1 - a_2^2)}{3 \times 2^{2/3} Z^{1/3}} - \frac{(1 - i\sqrt{3})Z^{1/3}}{6 \times 2^{1/3}} \tag{1.14}$$

$$x_3 = -\frac{a_2}{3} + \frac{(1 - i\sqrt{3})(3a_1 - a_2^2)}{3 \times 2^{2/3} Z^{1/3}} - \frac{(1 + i\sqrt{3})Z^{1/3}}{6 \times 2^{1/3}} \tag{1.15}$$

$$Z = -27a_0 + 9a_1a_2 - 2a_2^3 + 3\sqrt{3}\sqrt{27a_0^2 + 4a_1^3 - 18a_0a_1a_2 - a_1^2a_2^2 + 4a_0a_2^3} \tag{1.16}$$

where $i = \sqrt{-1}$. Each of these solutions may be real or complex depending on the values of the coefficients a_0, a_1, a_2. The expressions are finely balanced, and it is difficult to predict which of them will be real. $Z^{1/3}$ may become complex if $Z < 0$ or if the argument of the square root within Z becomes negative. The radicand[6] within Z is the cubic discriminant Eq. 1.18. Thus, as λ is scanned, the real root may switch between the three solutions x_1, x_2, x_3. In our case, the coefficients are $[a_0 = -4\rho,\ a_1 = 4[\lambda^2 + \epsilon^2(1 + \lambda)],\ a_2 = -4\lambda,\ a_3 = 1]$. All are small quantities, and therefore any Maclaurin series expansion (in which one variable is considered much smaller than another) is ruled out. We have to accept that trying to find, simplify or manipulate these roots analytically is a fools errand - except in special or contrived cases. Fortunately, some tricks (see below) have been developed to avoid evaluating the formal solutions.

Because it signals the presence of jump phenomena, the case of roots R_ρ all real is of particular interest. The condition for this is the cubic discriminant:

$$4(a_2^2 - 3a_1a_3)^3 \geq (2a_2^3 - 9a_1a_2a_3 + 27a_0a_3^2)^2 \ . \tag{1.17}$$

[6]The radicand is the expression or value inside a square root.

Substitution of the coefficients leads to:

$$8\lambda[\lambda^2 + 9\epsilon^2(1+\lambda)]\rho \geq 16\epsilon^2(1+\lambda)[\lambda^2 + \epsilon^2(1+\lambda)]^2 + 27\rho^2 \ . \tag{1.18}$$

Clearly $\lambda \times \rho > 0$. Taking the equality, and solving for λ generates the jump frequencies for given (ϵ, ρ). Unfortunately, this is a quintic equation for λ; and in general only one root is guaranteed to be real. Sorting through the five roots, and dismissing the complex ones, is tiresome. Nevertheless, Worden[22] has obtained these values numerically, and tabulated them for a sparse grid of (ϵ, ρ) values. For the jump-up frequency, which is always closer to the zero-amplitude resonance frequency, $(1+\lambda)$ may be replaced by 1; in this approximation, the quintic reduces to a quartic $8\lambda(9\epsilon^2+\lambda^2)\rho + 27\rho^2 \geq 16\epsilon^2(\epsilon^2+\lambda^2)^2$. The equality typically has two real and two complex roots; and one must choose between the two reals.

1.2.3 Resonance envelope

The envelope of all possible resonance curves, for a particular value of ρ, is given by the case $\epsilon = 0$. With no damping term, there is no resonance maximum (it is unlimited) and there is no upper turning point (location where $d\omega/dR = 0$). The cubic equation and its roots for R_ρ are simplified. Thus $R_\rho^3 - 4R_\rho^2\lambda + 4R_\rho\lambda^2 - 4\rho = 0$ and $Z \to 4[-4\lambda^3 + 27\rho + 3\sqrt{3}\sqrt{\rho(27\rho - 8\lambda^3)}]$.

Substituting $\epsilon = 0$ in the discriminant Eq. 1.18 leads to the condition $(2\lambda_c)^3 = 3^3\rho$. When $\rho > 0$, there is a single real root below the critical $\lambda_c = \frac{3}{2}\rho^{1/3}$; and three real roots above. With no damping term, there is no bound on the two large real roots when λ is progressively increased above λ_c. At λ_c, the roots are given by $(R_\rho - 4\rho^{1/3})(R_\rho - \rho^{1/3})^2 = 0$. λ_c is the lower turning point; it both bounds and is close to all the others when $\epsilon \neq 0$.

1.2.4 Branch points

Branch points are those where the sheets of a multi-valued function come together. The solution of the cubic equation is a multi-valued function $R_\rho(\lambda)$. The cubic has three solutions: either three real, or one real and two complex. At the branch points, either two of the three real solutions become equal, or two complex roots become equal pure real. At a branch point $d\lambda/dR_\rho = 0$; and a plot of $R_\rho(\lambda)$ is locally vertical.

There are always three solutions, $x_{1,2,3}$. However, we are interested only in the case of pure real roots; and shall restrict the meaning of "branches" and branch-points to the case of R_ρ real. A single root $R^2 > 0$ for all λ yields a single branch. When there are three positive roots, over a range of λ, we call the largest value the upper branch, the smallest value the lower branch, and the third value the middle branch.

There are frequencies where the real branch switches between the solutions x_1, x_2, x_3, say x_i before and x_j after the switch. But these are not branch points because $x_i \neq x_j$ at the switch point. Instead, the parties x_i, x_j are discontinuous about the switch point. Nevertheless, because the radicand appearing in Z is the cubic discriminant, two of the switching points coincide with the branch points. The switching behaviour is demonstrated in Fig. 1.1.

1.2.5 Far from resonance

For the small-amplitude tails far from resonance, approximations may be employed. In the regime $|R_\rho| \ll 1$ and $\sigma = 0$, Eq. 1.12 shrinks from a cubic to a quadratic condition in R_ρ with solution

$$R_\rho = [\theta - \sqrt{\theta^2 - 4\lambda\rho}]/\lambda \quad \text{where} \quad \theta \equiv \lambda^2 + \epsilon^2(1+\lambda) \ . \tag{1.19}$$

When $\rho > 0$, the ranges of applicability are $\lambda < -\epsilon$ and $(\theta^2 \geq 4\lambda\rho \ \& \ \lambda > 0)$. When $\rho < 0$, the valid ranges are $\lambda > \epsilon$ and $(\theta^2 \geq 4\lambda\rho \ \& \ \lambda < 0)$. The equality $\theta^2 = 4\lambda\rho$ provides an estimate of the jump-up frequency; because at this value $dR_\rho/d\lambda \to \infty$. Unfortunately, this is a quartic equation for λ. Before the jump, the value $R_\rho \approx \sqrt{\rho/\lambda}$.

Asymptotic values

In the limit of very small R_ρ, the response is $R^2 = 1/[\lambda^2 + \epsilon(1+\lambda)]$. And in the limit of very large λ, the asymptotic limit is $R_\rho \to \rho/\lambda^2$.

1.2.6 Response at DC

From Eq. 1.8, the response is $R^2 = 1/[\epsilon^2(1+\lambda) + (\lambda - R_\rho/2)^2]$. At D.C. we insert $\lambda = -1$ on the right. The response becomes self-consistent when we replace R^2 with R_ρ/ρ on the left of the equality. Thus results a cubic equation $R_\rho/\rho = 1/(1 + R_\rho/2)^2$. This has the solution Eq. 1.16 with coefficients $a_i = c_i/c_4$ and $[c0, c1, c2, c3, c4] = [1, 4, 4, -4\rho]$. If $\rho > 0$, only the first branch is real. If $\rho < 0$ there are three real solutions, provided $\rho > \rho_0 \equiv -(2/3)^3$. At the ends of the range $\rho_0 \le \rho \le 0$, two solutions coalesce leaving $R_\rho(\rho = 0) = [0, -2]$ and $R_\rho(\rho = \rho_0) = [-2/3, -8/3]$. Over the entire range ρ positive or negative, the first branch is real and approximates to $R_\rho \approx \rho$. Hence, at D.C. $R^2 \approx 1$.

1.2.7 Resonance locus

The "trick" to tracing out the resonance is to write (R_ρ, λ) in terms of a parameter, and then to sweep this parameter to generate the resonance curve. Such a curve is called a *locus*. The slew rate must be zero: $\sigma = 0$. The trick comes in two varieties. The first relies on a self-consistency argument. The second relies on inversion of the cubic equation for λ as a function of R_ρ. For both types, there is nothing more complicated than quadratic equations and square roots. The starting point for the first variety is the resonance equation:

$$R^2 = \frac{4}{4(\epsilon w)^2 + (2 + R^2\rho - 2w^2)^2} \;=\; \frac{4}{4\epsilon^2(1+\lambda) + (R_\rho - 2\lambda)^2} \; . \tag{1.20}$$

We introduce the parameter a as the solution of $(R_\rho - 2\lambda) + a = 0$; or $\lambda = (a + R_\rho)/2$. As a increases, we sweep-up across the resonance. We insert the parametrised λ into the resonance expression yielding $R^2 \equiv R_\rho/\rho = 4/[a^2 + 4\epsilon^2 + 2(a + R_\rho)\epsilon^2]$. This is the self-consistency condition. It is a quadratic equation to be solved for R_ρ. We take the root with $\rho \times R_\rho > 0$. The self-consistent R_ρ is then substituted (trivially) into λ so that this also becomes consistent. Define $\theta = a^2 + 2(a+2)\epsilon^2$. The expressions are:

$$R_\rho = [-\theta + \sqrt{\theta^2 + 32\epsilon^2\rho}]/(4\epsilon^2) \quad \text{and} \quad \lambda = (a + R_\rho)/2 \; . \tag{1.21}$$

a is swept from negative to positive values to generate the locus $[\lambda(a), R_\rho(a)]$ for fixed (ϵ, ρ). The non-linear relation between R_ρ and a has the effect (nonlinear shear) of removing the tilt from the resonance curve. If $R_\rho(\lambda)$ is multi-valued, and a is monotonic increasing, then $\lambda(a)$ will pass (continuously) along all branches of the resonance curve; to omit the middle branch, a range of a values must be omitted. This locus is a valuable tool, and will be used in Secs. 1.3 and 1.5.3. Alternatively, for special values of a, we may generate curves as a function of ϵ or ρ.

Limiting value of $\rho < 0$

For the softening oscillator, $\rho < 0$, the radicand (in Eq. 1.21) may become negative; and this leads to a constraint on the combinations of (ϵ, ρ) for which a steady state may exist. The absence of an SS indicates the system is unstable. The condition $\theta^2 - 32\epsilon^2|\rho| > 0$ is satisfied by $[a > 0 \;\&\; 0 < \epsilon < \sqrt{2} \;\&\; 2|\rho| < \epsilon^2]$ or by $a < 0$ and

$$0 < \epsilon < \sqrt{2} \quad \text{and} \quad |\rho| < \epsilon^2(1 - \epsilon^2/4)^2/2 \; . \tag{1.22}$$

The latter case gives the stability limit when $\rho < 0$.

Resonance maximum $\hat{R}_\rho$

The resonance is limited by dissipation. At the maximum of the response curve, $dR^2/d\lambda = 0$ where R^2 is given by Eq. 1.20. This has solution $2\lambda = R_\rho - \epsilon^2$. We may consider the equivalent $dR_\rho/da = 0$, which has solution $a = -\epsilon^2$, leading to $\hat{R}_\rho = 2\lambda_r + \epsilon^2$. This relation is often called the backbone or spine; and it means that if we find any pairs $(\lambda_r, \hat{R}_\rho)$, by another method, they will satisfy the spine condition. To find an explicit expression, we must substitute the special value $a = -\epsilon^2$ into Eq. 1.21 to find the function $\hat{R}_\rho(\epsilon, \rho)$.

Explicitly, the spine is $\quad 2\lambda_r = \hat{R}_\rho - \epsilon^2 \quad$ and $\quad \hat{R}_\rho = \sqrt{(1-\epsilon^2/4)^2 + 2\rho/\epsilon^2} \; - (1 - \epsilon^2/4)$. (1.23)

The expression is valid for $0 < \rho < 2$, or Eq. 1.22 when $\rho < 0$; and $\epsilon < 2$ always.

Note, some authors are careless with notation: they state that the backbone is $2\lambda = R_\rho - \epsilon^2$ without clarifying that R_ρ must be a solution of the cubic. It is better to write the spine as $2\lambda = \hat{R}_\rho(\epsilon, \rho) - \epsilon^2$. Even more careless is to state that the backbone is $2\lambda = R_\rho$, because this confuses the maximum with the linear-instability theshold.

Linear-Instability threshold

Another special value is $a = 0$. This generates a pair $(\lambda_s, R_{\rho\, s})$ that lies between the maximum and the jump-down location $(\lambda_u, R_{\rho\, u})$. All three points lie close together on the resonance curve. This special value is

$$2\lambda_s = R_{\rho\, s} \quad \text{and} \quad R_{\rho\, s} = \sqrt{1 + 2\rho/\epsilon^2} - 1 \; . \tag{1.24}$$

At this location, the real part of the complex oscillation frequency for small perturbations is identically zero. This is the kind of instability that may occur in a linear system of two coupled oscillators. There is a second special value $(\lambda_t, R_{\rho\, t})$ at which small perturbations cease to be damped; it is the solution of $2\lambda = 3R_\rho$.

1.2.8 Resonance curve

The second"trick" is to recognize[3, 10, 15] that the oscillator response Eq. 1.12 is a cubic in R_ρ but a quadratic in λ. Mathematically, an equation is an equivalence between the quantities therein; and Eq. 1.12 may be solved for either $R_\rho(\lambda)$ or $\lambda(R_\rho)$. Physically, time ordering is lost in the steady state because there are no dynamical effects; and so the equation may be solved for the excitation frequency as a function of the response.

The starting point for the second parametrization is the cubic Eq. 1.12 with $\sigma = 0$. This is solved for λ, yielding

$$2\lambda_\pm = (R_\rho - \epsilon^2) \pm \sqrt{R_\rho[R_\rho\epsilon^2(-4 + \epsilon^2 - 2R_\rho) + 4\rho]}/R_\rho \; . \tag{1.25}$$

Both solutions are needed. The amplitude R_ρ is dual-valued on the branch λ_+, and single valued on λ_-. The locus is formed by plotting the coordinate pairs (λ_-, R_ρ) and (λ_+, R_ρ) as R_ρ is scanned from near-zero to its maximum value $\hat{R}_\rho$ given by the zero of the radicand. At this value, the two branches $\lambda_\pm$ become equal, and this corresponds to the maximum of the resonance. The construction is shown below, Fig. 1.4.

Resonance maximum

$\hat{R}_\rho$ is a solution of $R_\rho \times (\epsilon^2 - 4 - 2R_\rho) + 4\rho = 0$. This is a quadratic with two solutions:

$$\hat{R}_\rho = -(1 - \epsilon^2/4) \; \pm \sqrt{(1-\epsilon^2/4)^2 + 2\rho/\epsilon^2} \; . \tag{1.26}$$

The maximum occurs on the upper branch with the positive sign before the radical. This value is inserted into the expression (1.25) for $\lambda(R_\rho)$, yielding the frequency at the maximum $\lambda_r = \lambda_- = \lambda_+ = (2\hat{R}_\rho - \epsilon^2)/2$. Note, $(\lambda_r, \hat{R}_\rho)$ is not the location of the jump-down point, but it is close to it.

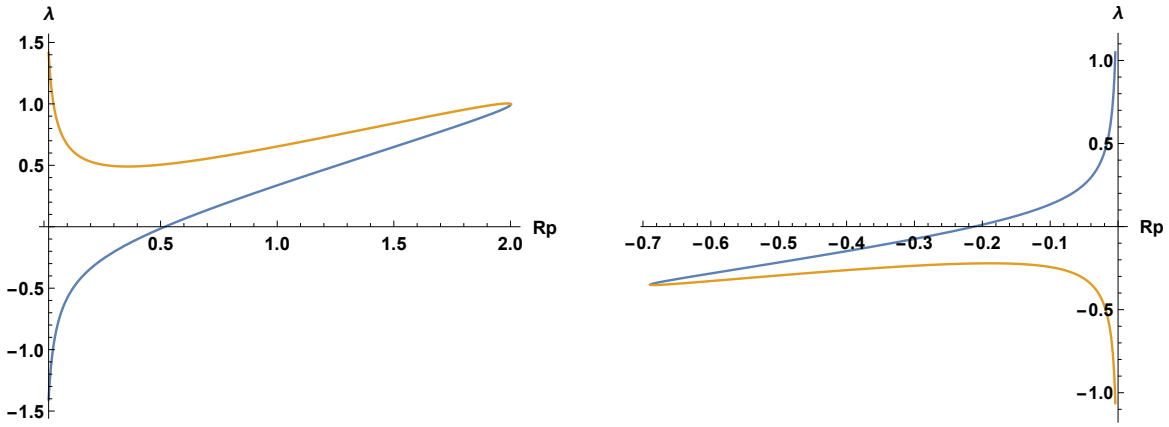

Figure 1.4: Resonance curve construction with parameter R_ρ. Upper branch λ_- shown gun-blue, lower/middle branch λ_+ shown gold. Left ($\epsilon = 0.1, \rho = 0.04$). Right ($\epsilon = 0.1, \rho = -0.0045$).

Limiting value of $\rho < 0$ and cusp

Stability conditions for the softening oscillator are more complicated, because the restoring force passes through zero and goes negative for sufficiently large amplitudes. This may occur (if ρ is too negative) before the resonance amplitude is limited by dissipation. When $\rho < 0$, we must plot $(\lambda_\pm, -R_\rho)$. The behaviour is qualitatively different because now the radicand (in Eq. 1.25) is $R_\rho(\epsilon^2 - 4 - 2R_\rho) - 4|\rho| = 0$. This is positive provided that $[0 < \epsilon < 2 \;\&\; -\epsilon^2(1-\epsilon^2/4)^2/2 < \rho < 0]$. If ρ violates this condition then λ becomes complex, and there are no steady state solutions. This confirms the result (1.22) above.

At the limiting value of ρ, the radicand (in Eq. 1.26) is zero yielding the response maximum

$$R^2 \times \rho = \hat{R}_\rho = -(1 - \epsilon^2/4), \quad 2\lambda_r = -(1 + 3\epsilon^2/4) \quad \text{and} \quad \rho < 0\,. \tag{1.27}$$

There is a jump-down frequency λ_u and a linear instability frequency λ_s. Typically, they both lie at frequency just below λ_r. However, at the limiting ρ all three frequency values merge. In such a case, the resonance curve ends is a horn or cusp[7] - rather than smoothly folding over to lower values. And, in this case, Eq. 1.27 becomes the jump-down condition.

1.2.9 Turning points

Turning points (TP) are an alternative name for the branch points. There are two ways to find the TPs: from the cubic discriminant (Eq. 1.18), or as follows. The jumps take place in the immediate neighbourhood of the turning points; these are locations where the derivative dw/dR^2 or $d\lambda/dR_\rho$ is locally zero; or equivalent dR^2/dw and $dR_\rho/d\lambda$ have poles. The locations are coordinate pairs $(\lambda_l, R_{\rho\,l})$ for the lower, and $(\lambda_u, R_{\rho\,u})$ for the upper turning point.

We shall use the methods introduced in Secs. 1.2.7 and 1.2.8 to find the critical value of ρ for the emergence of two branch points. We find two expressions, one for the zero of $d\lambda/dR_\rho$ and another from $\lambda(R_\rho)$, and tie them together to find the threshold $\rho(\epsilon)$. At precisely the point of emergence, the branch points are equal and R_ρ is single valued. Above this critical value, R_ρ becomes triple valued.

Starting from the cubic (Eq. 1.12) , we form the implicit derivative:

$$\frac{d}{dw}R^2 = \frac{8wR_\rho(R_\rho - 2\lambda - \epsilon^2)}{[3R_\rho^2 - 8Rp\lambda + 4(\lambda^2 + \epsilon^2(1+\lambda))]\rho}\,. \tag{1.28}$$

[7]The derivative $d\lambda/dR_\rho$ is discontinuous: it changes sign without passing through zero.

The zero of the numerator gives a condition for $\hat{R}_\rho$. The zero of the denominator (or pole) gives a condition for the turning point. This is a quadratic equation, and can be solved for either λ or R_ρ. Solving for the latter leads to a simpler form:

$$(3/2)R_\rho = 2\lambda \pm \sqrt{\lambda^2 - 3\epsilon^2(1+\lambda)}\ . \tag{1.29}$$

Relation 1.29 is given by Asok[11] Sec. 6.4.1, albeit in a different notation. The relation means that if we have a set of TPs, for differing (ϵ, ρ), they will all lie on the locus. If, by some means, we find one of the pair (λ, R_ρ), then the other is supplied by the relation. But pairs cannot be freely chosen according to Eq. 1.29, they are constrained to satisfy the cubic equation Eq. 1.12. Nevertheless, the relation does enshrine a remarkable property. At the threshold ρ for emergence of turning points, all the λ are the same (depend only on ϵ), and the pair will always be in the relationship $R_\rho = (4/3)\lambda$. The threshold depends on the values of (ϵ, ρ) and will be found below.

Emergence of TPs

The positive/negative sign before the radicand gives the upper/lower turning point. The turning points meet (emerge) when the radicand is zero, and two roots become equal; and R_ρ becomes $R_\rho = (4/3)\lambda$. The roots of the radicand are

$$\lambda = (3/2)\epsilon^2 \pm \epsilon\sqrt{3}\sqrt{1 + (3/4)\epsilon^2}\ . \tag{1.30}$$

The positive/negative sign before the radicand gives the threshold for the hardening/softening resonator. When the turning points emerge, $\lambda_l = \lambda_u$, this is the value of λ and $R_\rho = (4/3)\lambda$. We take this a step further. From the cubic, we have the self-consistency condition $R_\rho = 4\rho/[(R_\rho - 2\lambda)^2 + 4\epsilon^2(1+\lambda)]$. We substitute $(4/3)\lambda$ in place of R_ρ, leading to a cubic equation that determines the emergence value of λ, namely $4\lambda = 27\rho/[\lambda^2 + 9\epsilon^2(1+\lambda)]$.

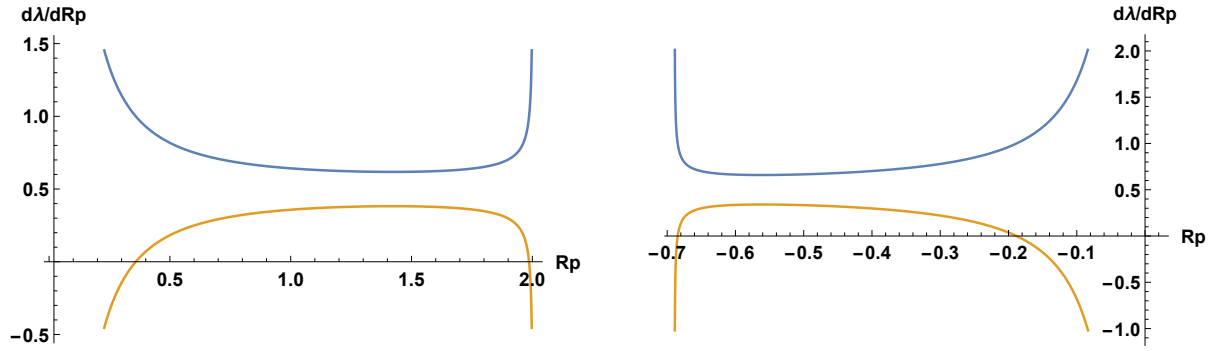

Figure 1.5: Derivative of resonance curve versus parameter R_ρ. Upper branch λ_- shown gun-blue, lower/middle branch λ_+ shown gold. Left $(\epsilon = 0.1, \rho = 0.04)$. Right $(\epsilon = 0.1, \rho = -0.0045)$.

Critical value of ρ

But we still do not yet know the critical value of ρ at which the threshold occurs. The self-consistent condition is cubic in ρ and quadratic in λ. The second point of departure is the two solutions for λ. We encountered them before, Eq. 1.25. Both solutions are needed, and the radicand Z sets the permissible range of R_ρ. We form the derivative with respect to λ, thus

$$\frac{d\lambda}{dR_\rho} = \frac{2R_\rho\sqrt{Z} \pm (R_\rho^2\epsilon^2 + 2\rho)}{R_\rho\sqrt{Z}}\ , \qquad Z = R_\rho[R_\rho\epsilon^2(-4 + \epsilon^2 - 2R_\rho) + 4\rho]\ . \tag{1.31}$$

Both values are legitimate. With the positive sign, the derivative is single-signed and refers to the upper branch. With the negative sign, the derivative is dual-signed and refers to the middle and lower branches where the turning points lie; see Fig. 1.5. We take the negative sign and equate $d\lambda/dR_\rho$ to zero, yielding the quintic condition:

$$2R_\rho^4(2+R_\rho)\epsilon^2 \; + 4R_\rho^2(\epsilon^2 - R_\rho)\rho \; + 4\rho^2 = 0\,. \tag{1.32}$$

Notice that it is quadratic in ρ. We substitute the emergence conditions: first that $R_\rho = (4/3)\lambda$, and second the two values of λ Eq. 1.30. The smaller/larger λ leads to a threshold condition for the softening/hardening oscillator. We solve the quadratic for ρ. There are two solutions for each λ value. By inspection, we pick a single solution for each regime ($\rho < 0$) or ($\rho > 0$). For brevity, let $p \equiv \sqrt{12+9\epsilon^2}$ and $q \equiv (4+3\epsilon^2)$. The expressions, valid for $\epsilon \leq 2$, are exact but lengthy:

$$\rho \;=\; (4/9)\epsilon^3\left\{-4p + 3\epsilon(10 - 3p\epsilon + 9\epsilon^2) + \sqrt{6}\sqrt{q[2+\epsilon(-2p+3\epsilon(q-p\epsilon))]}\right\},\quad \rho<0 \tag{1.33}$$

$$\rho \;=\; (4/9)\epsilon^3\left\{+4p + 3\epsilon(10 + 3p\epsilon + 9\epsilon^2) - \sqrt{6}\sqrt{q[2+\epsilon(2p+3\epsilon(4+\epsilon(p+3\epsilon)))]}\right\},\quad \rho>0 \tag{1.34}$$

Relations 1.34 and 1.34 are new. When $\epsilon \ll 1$, we truncate them in a power series:

$$\rho \;\approx\; \frac{4}{9}\epsilon^3\left[-4\sqrt{3} \; + 18\epsilon \; - (27\sqrt{3}/2)\epsilon^2 \; + 18\epsilon^3 + \ldots\right],\quad \rho<0 \tag{1.35}$$

$$\rho \;\approx\; \frac{4}{9}\epsilon^3\left[12\sqrt{3} \; + 42\epsilon \; + (57\sqrt{3}/2)\epsilon^2 \; + 36\epsilon^3 + \ldots\right],\quad \rho>0\,. \tag{1.36}$$

Often the approximate critical values $\rho \approx 16\epsilon^3/\sqrt{3} > 0$ and $\rho \approx -16\epsilon^3/(3\sqrt{3}) < 0$ will suffice.

Explicit TP locations

In the preceding subsection we have found conditions for the turning points, but not the TP values themselves. In general, we have to accept that having accurate values for the location of turning points is more important than having analytic expressions; and there is no choice but to solve the quintic equations exactly. Either Eq. 1.18 for λ or Eq. 1.32 for R_ρ. Let us rewrite the latter quintic as $\sum_{n=0}^{5} a_n R_\rho^n$. The coefficients are $[a_0, a_1, a_2, a_3, a_4, a_5] = [1, 0, 2/\chi, -1/\rho, 2/(\rho\chi), 1/(\rho\chi)]$ which serves to emphasize the import role of the dimensionless groups ρ and χ.

1.3 Linear Stability Analysis

We found the steady state solutions in Sec. 1.2. We now consider the stability of small perturbations. We take a trial solution $y(z) = A\times[1+a(z)]\cos\phi + B\times[1+b(z)]\sin\phi$, where A, B are constant, and the modulations $a(z)$ and $b(z)$ are considered slowly varying compared with the phase advance $\phi(z)$. $\phi = wz$ at fixed drive or $\phi = wz + \sigma z^2/2$ if the drive frequency is swept. The trial is inserted in the EOM 1.3. We take $\langle y^2\rangle$ to be $A^2(1+a)^2/2 \; + B^2(1+b)^2/2$; and we linearize in a and b. As before we employ the principle of harmonic balance, and compare the coefficients of $\cos\phi$ and $\sin\phi$. We subtract off the steady state conditions Eq. 1.6, leaving coupled equations for the modulations:

$$(1/2)A(2+3A^2\rho + B^2\rho - 2w^2)a(z) + B(AB\rho + \sigma + \epsilon\, w)b(z) + A\epsilon\, a' + 2Bwb' + Aa'' \;= 0 \tag{1.37}$$

$$A(AB\rho - \sigma - \epsilon\, w)a(z) + (1/2)B(2+A^2\rho + 3B^2\rho - 2w^2)b(z) - 2Awa' + B\epsilon\, b' + Bb'' \;= 0 \tag{1.38}$$

We make the Laplace transform with respect to complex frequency s, such that $a(z) \to a(s)$, $a'(z) \to sa(s)$, $a''(z) \to s^2a(s)$; and likewise for $b(z)$. The resulting equations are written in matrix form $\mathbf{Mx} = \mathbf{0}$ where the vectors $\mathbf{x} = [a(s), b(s)]$ and $\mathbf{0} = [0, 0]$; and the matrix is

$$\mathbf{M} = \begin{bmatrix} As^2 + As\epsilon + A(2+3A^2\rho + B^2\rho - 2w^2)/2 & 2Bsw + B(AB\rho + \sigma + \epsilon\, w) \\ -2Asw + A(AB\rho - \sigma - \epsilon\, w) & Bs^2 + Bs\epsilon + B(2+A^2\rho + 3B^2\rho - 2w^2)/2 \end{bmatrix}$$

The equation $\mathbf{Mx} = \mathbf{0}$ has non-trivial solutions if the matrix determinant is identically zero. This determinant is $AB(c_0 + c_1 s + c_2 s^2 + c_3 s^3 + c_4 s^4)$ where the coefficients are

$$c_0 = \left\{ R_\rho(8 + 3R_\rho) - 8R_\rho w^2 + 4w^4 + 4[1 + \sigma^2 + 2\,\epsilon\,\sigma\,w - (2 - \epsilon^2)w^2] \right\}/4 \tag{1.39}$$

$$c_1 = 2[2\sigma\,w + \epsilon(1 + R_\rho + w^2)], \quad c_2 = \epsilon^2 + 2(1 + R_\rho + w^2), \quad c_3 = 2\epsilon, \quad c_4 = 1\ . \tag{1.40}$$

We rewrite the coefficients in terms of $w^2 = 1 + \lambda$, thus:

$$c_0 = (3/4)R_\rho^2 - 2R_\rho\lambda + \lambda^2 + \epsilon^2(1 + \lambda) + \sigma^2 + 2\epsilon\sigma\,w \tag{1.41}$$

$$c_1 = 2\epsilon(2 + R_\rho + \lambda) + 4\sigma\,w, \quad c_2 = \epsilon^2 + 2(2 + R_\rho + \lambda), \quad c_3 = 2\epsilon, \quad c_4 = 1\ . \tag{1.42}$$

The combinations of (R_ρ, λ) appearing here satisfy the steady state condition Eq. 1.12. In principle, we could use the Routh-Hurwitz criteria (for a quartic) to determine conditions that the roots s have negative real part, indicating damping and stability.

However, the coefficients c_2, c_3, c_4 are so simple they inspire us to believe the form of the roots can be guessed when the coupling term σ is set to zero. Let $i = \sqrt{-1}$. We take the trial form $D = (s + \epsilon/2 + p)(s + \epsilon/2 - p)(s + \epsilon/2 + iq)(s + \epsilon/2 - iq)$ where p, q are real and initially unknown. We shall equate the coefficients of s^0, s^1, s^2, s^3, s^4 appearing in D to the corresponding coefficients c_0, c_1, c_2, c_3, c_4. The conjugate roots imply that p and q will only ever appear as their squares, $P = p^2$ and $Q = q^2$. Consequently, the onset of instability is signaled either by P being positive and $\sqrt{P} \geq \epsilon/2$, or by Q becoming negative and $\sqrt{|Q|} \geq \epsilon/2$. $P < 0$ is not a problem, because it corresponds to a damped oscillation. There are two simultaneous equations:

$$P - Q + 2[R_\rho + (2 + \lambda) - \epsilon^2/4] = 0, \quad (4P - \epsilon^2)(4Q + \epsilon^2) + 4(R_\rho - 2\lambda)(3Rp - 2\lambda) = 0\ . \tag{1.43}$$

There are precisely two solutions: (P_+, Q_+) and (P_-, Q_-) where

$$P_\pm = -(2 + R_\rho - \epsilon^2/4 + \lambda) \pm (1/2)\sqrt{R_\rho^2 + 16(1 + \lambda)(1 + R_\rho)} \tag{1.44}$$

$$Q_\pm = +(2 + R_\rho - \epsilon^2/4 + \lambda) \pm (1/2)\sqrt{R_\rho^2 + 16(1 + \lambda)(1 + R_\rho)}\ . \tag{1.45}$$

Given that $R_\rho > 0$ for the hardening oscillator, and $R_\rho < 0$ for the softening resonator, their behaviours will be very different. A non-zero value of σ will break the degeneracy; the real and imaginary parts become split (i.e raised or lowered), but the effect is small.

There may be instability if Q_- is sufficiently negative, or P_+ is sufficiently positive; in fact they are the same condition. So we need only to consider the first couplet (P_+, Q_+). As it transpires, $Q_+ > 0$ always. The threshold occurs when the net growth rate exceeds zero, that is when $P_+ > \epsilon^2/4$. Going forward, we drop the subscript '+'.

We consider the properties of P and Q. At DC, $\lambda = -1$ and $R_\rho \approx \rho$; and thus $P = -1 + \epsilon^2/4 - \rho/2$ and $Q = 1 - \epsilon^2/4 + 3\rho/2$. Here $P < 0$ and $Q > 0$, so there is no instability. At large frequency, $\lambda \gg 1$ we take $R_\rho \to \rho/\lambda^2$, and find the asymptotic limit

$$P \to -2 + \epsilon^2/4 - \lambda + 2\sqrt{\lambda} \quad \text{and} \quad Q \to +2 - \epsilon^2/4 + \lambda + 2\sqrt{\lambda}\ . \tag{1.46}$$

Here $P < 0$ and $Q > 0$, so there is no instability.

1.3.1 Locations of thresholds

Evidently, positive growth rates are ruled out except in the vicinity of resonance. We can narrow this down. The threshold condition $\sqrt{P} > \epsilon/2$ implies

$$8 - 4R_\rho + \epsilon^2 - 4\lambda + 2\sqrt{R_\rho^2 + 16(1 + \lambda)(1 + 16R_\rho)} \geq \epsilon^2\ . \tag{1.47}$$

When $[\lambda > 0, R_\rho > 0, \epsilon > 0]$, this is satisfied for $R_\rho \leq 2\lambda \leq 3R_\rho$. Here (λ, R_ρ) must be a solution of the cubic Eq. 1.12. We examine this regime by use of the parametrization $2\lambda = R_\rho + \epsilon\, b$ and scanning b. Here $R_\rho(b) = [-(4 + b^2 + 2b\epsilon) + \sqrt{(4 + b^2 + 2b\epsilon)^2 + 32\rho/\epsilon^2}]/4$.

At the lower limit ($\lambda = R_\rho/2$) Eq. 1.47 is satisfied by $b = 0$. Hence at the special point Eq. 1.24, one root becomes $s = 0$; and stability is lost.[8] At the upper limit ($\lambda = 3R_\rho/2$) this leads to a cubic condition $(8\rho)/\epsilon^2 = b\epsilon(4 + b^2 + 3b\epsilon)$ which has at least one real root b. At this cubic root $P = \epsilon^2/4$, and one root of the determinant becomes $s = 0$. Between the limits $R_\rho \leq 2\lambda \leq 3R_\rho$, P is approximately parabolic with a maximum. Hence there is always a range of values λ over which the instability threshold is exceeded, provided only $\rho > 0$. For sufficiently small ρ that the resonance curve does not fold over, the solution is roughly $b \approx 2\rho/\epsilon^3$ with the caveat $b \leq 1$. In this regime, the unstable range is narrow and the net growth rate a small fraction of $\epsilon/2$. When ρ is sufficiently large that the resonance curve is clearly multi-valued, the solution is $b \approx (2\rho)^{1/3}/\epsilon$ with the caveat $b > 4$. Such values lie on the lower branch and close to $(\lambda_l, R_{\rho l})$. In this regime, the unstable range extends slightly beyond the (lower and upper) limits of the middle branch. Outside the middle branch, the net growth rate is small. On the middle branch, the growth rate may rise to large values; but the oscillator never accesses the middle branch. This is as far as we can get with analysis, the rest is up to numerics.

We have sampled ϵ and ρ, and for each case have scanned P, Q as a function of $a = b\epsilon$. All confirm the assertions above. A subset is shown in the following examples, Fig. 1.6 and Fig. 1.7. The plots show $\text{sign}[P]\sqrt{|P|}/(\epsilon/2)$ and $\sqrt{Q}$ values (gun-blue and gold, respectively) across the resonance. Superimposed, to guide the eye, is the resonance curve shown blue. That part of the curve that lies between λ_l and λ_u, the middle branch is shown red. Also shown, and relevant only to P, is the instability threshold $P/(\epsilon^2/4) = 1$ drawn in light green. Crucially, the plots confirm that the range of values over which the threshold is exceeded is slightly wider than the range $[\lambda_l, \lambda_u]$; and that such a range (albeit small) exists even when R_ρ is single-valued.

In summary, there are positive growth rates on the entire middle branch; and they may be large. But the resonator state never falls on the middle branch. There are also growth rates on a tiny portion of the upper and lower branches close to the branch points; but these rates are very small. When there are no branch points, but ρ is non-zero, there are very small growth rates for a narrow band of frequency just beyond the maximum response. Although the value of the anti-damping is small a (fraction of ϵ) on the upper and lower branches, it may be argued that due to the very slow sweep rate, the drive frequency may hover around these conditions for many e-folding times.

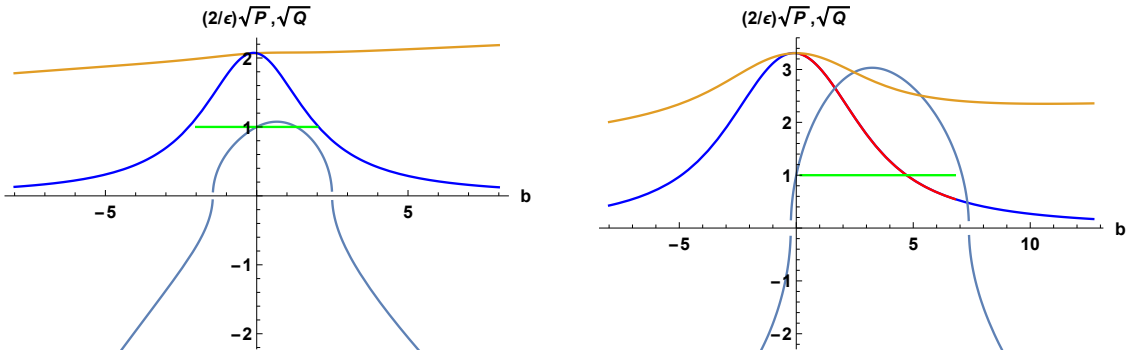

Figure 1.6: Stability plot for hardening resonator. Loci of $\sqrt{P}$ (gun-blue), $\sqrt{Q}$ (gold), resonance curve (blue), threshold (green). Left: single-valued ($\epsilon = 0.1, \rho = +0.001$). Right: multi-valued ($\epsilon = 0.1, \rho = 0.05$).

[8] The limiting form of $\exp(st)$ as $s \to 0$ is growth linear proportional to time t, which is unbounded. This is sometimes called a monotonic instability.

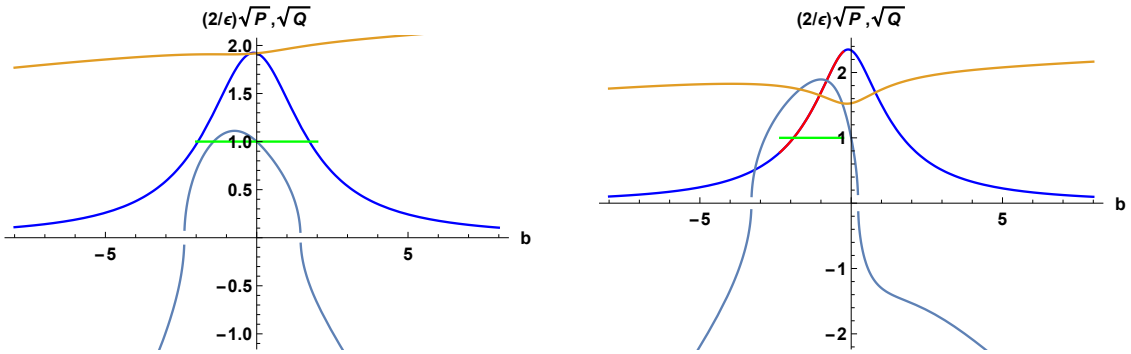

Figure 1.7: Stability plot for softening resonator. Loci of $\sqrt{P}$ (gun-blue), $\sqrt{Q}$ (gold), resonance curve (blue), threshold (green). Left: Single-valued ($\epsilon = 0.1, \rho = -0.001$). Right: multi-valued ($\epsilon = 0.1, \rho = -0.004$)

1.4 Dynamics Dominated Regime

Given that the mean-square resonator (and the Duffing resonator) may have multiple steady-state solutions, it is evident that the uniqueness proof of Urabe must break down. It does so for two reasons. Firstly, Urabe relies on the convergence of Newton iterations; and this depend on the Jacobian matrix $\mathbf{M}$ (given in Sec. 1.3) for small (linear) perurbations. But the $s = 0$ solutions (which occur close to the TPs) of the characteristic determinant implies that $\mathbf{M}$ is not always invertible, and so iteration fails. Indeed, the $\Re[s] > 0$ solutions (that occur on the middle branch) implies that the iterations may diverge. Secondly, Urabe relies on all derivatives being bounded (finite); but that condition is violated precisely at the turning points where $d\omega/dR \to \infty$. It is this second failure that is explored in this section.

The assumption that the driven MSO or DO has a steady state is almost an act of faith. But for a damped system there is the hope[9] that when all transients have died away, the residual is periodic (sinusoidal for the MSO) and in lock-step with the drive. This hope is enshrined in the assumption that the amplitude derivatives $\dot{A}, \ddot{A}, \dot{B}, \ddot{B}$ are (at all times) much smaller than the damping rate. This is quantified by the inequalities: $|A'| \ll \epsilon A$ and $|B'| \ll \epsilon B$. If they are violated, then the assumptions are not self-consistent. [The primes denote derivatives $A' \equiv dA/dz$ with respect to the dimensionless time variable z; they are the rates per cycle of harmonic motion when $\rho = 0$.] Both quantities are related to R and R'. For the swept frequency drive, the normalized drive frequency is time varying, so we write $w \equiv w(z)$. For such a case we have quasi steady-state solutions for A, B, R and are thus equipped to test the inequalities based on $X' = (dX/dw)(dw/dz) = (dX/dw)\sigma$ where X is any of A, B, R, R^2 and the slew rate is $\sigma = \dot{\omega}/\alpha$; and $w(z) = w_0 + \sigma z$. Significantly, the sign (positive or negative) of X' is directly influenced by that of σ: and, therefore, the behaviour is markedly different between up and down sweeps.

As before, we shall write expressions in terms of the dimensionless variables ($w = \omega/\sqrt{\alpha}$, $z = t\sqrt{\alpha}$, etc) for simplicity and brevity. The starting point is Eq. 1.7, where we must write $A \equiv A(w)$, $B \equiv B(w)$ and $R \equiv R(w)$. We perform the derivative according to the chain rule, $X' = (dX/dw)(dw/dz) = (dX/dw)\sigma$, to find:

$$A'/\sigma = -2wR^2(w) + [1 - w^2 + \rho R^2(w)](dR^2/dw), \qquad B'/\sigma = \epsilon[R^2(w) + w(dR^2/dw)] \,. \tag{1.48}$$

The derivatives can be considered large if their moduli are greater than the damping rates, ϵA and ϵB. We now substitute the expression for dR^2/dw. Technically, we should take the derivative of $R(\epsilon, \rho, \sigma)$; but the position of the poles and zeroes of dR/dw is almost unshifted provided that $|\sigma|$ is small compared with ϵ; and setting $\sigma = 0$ will result in much simpler expressions for the derivatives

[9] Contrastingly, when $\delta = 0$ and the frequency is swept, a dynamic steady state is never achieved.

dX/dw. However, we always maintain a non-zero sweep rate; we do not set σ to zero ($\dot{\omega} \neq 0$). We start from the cubic equation $R^2(w)[(\epsilon w)^2 + (1 - w^2 + \rho\, R^2/2)^2] = 1$; and form the derivative:

$$\frac{d}{dw}R^2 = \frac{2wR^2(w)[2(1-w^2) - \epsilon^2 + \rho R^2]}{[(1-w^2)^2 + (\epsilon w)^2] + 2(1-w^2)\rho R^2 + (3/4)(\rho R^2)^2} \,. \tag{1.49}$$

Evidently, due to the product terms $R^2 \times R^2$, growth or decay may be faster than exponential. The expressions Eqs. 1.48 and 1.49 are simpler when written in terms of λ, R_ρ. For example,

$$\frac{d}{dz}R^2 = \sigma\frac{d}{dw}R^2 = \frac{\sigma\, 8R_\rho(R_\rho - 2\lambda - \epsilon^2)\sqrt{1+\lambda}}{[3R_\rho^2 - 8\lambda R_\rho + 4(\lambda^2 + \epsilon^2(1+\lambda))]\rho} \,. \tag{1.50}$$

The jump locations are the solutions of the denominator equal to zero. Some of their properties were described in Sec. 1.2.9

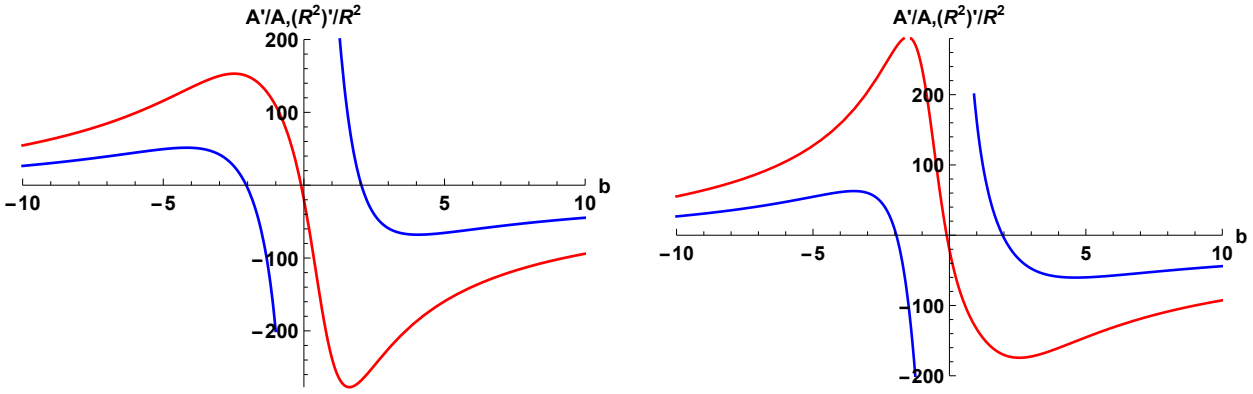

Figure 1.8: R_ρ Single-valued. A'/A shown blue, $\propto R'/R$ red. Left: hardening resonator ($\epsilon = 0.1, \rho = 0.001$). Right: softening resonator: ($\epsilon = 0.1, \rho = -0.001$).

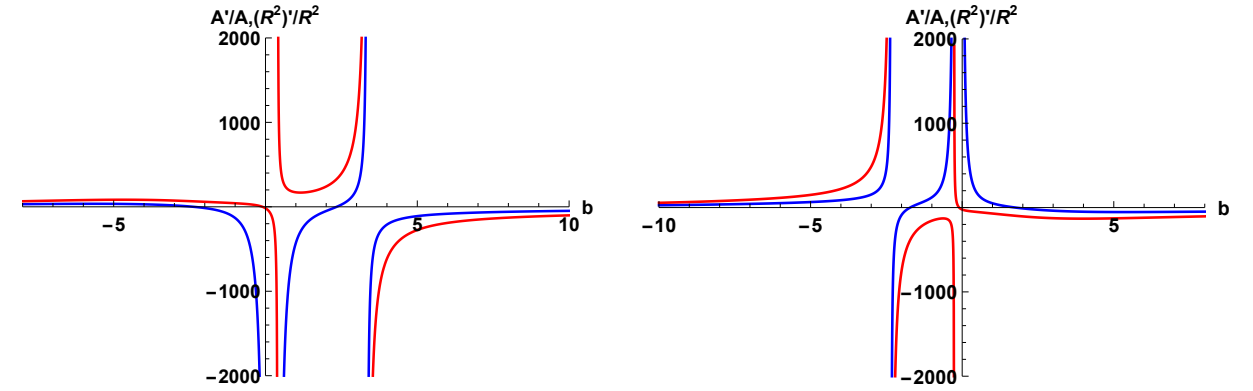

Figure 1.9: R_ρ Triple-valued. A'/A shown blue, $\propto R'/R$ red. The ordinate is artificially truncated at 2000. Left: hardening resonator ($\epsilon = 0.1, \rho = +0.01$); λ_u at $b \approx 0$, λ_l at $b \approx 3.5$. Right: softening resonator ($\epsilon = 0.1, \rho = -0.004$); λ_u at $b \approx 0$, λ_l at $b \approx -2.5$.

We now have all the ingredients (Eqs. 1.7, 1.48, 1.49) to form the quantities $\xi_A = (dA/dw)/(\epsilon A)$, $\xi_B = (dB/dw)/(\epsilon B)$, $\xi_R = (dR^2/dw)/(\epsilon R^2)$ and test the near-equilibrium conditions $|\xi_A\sigma| < 1$, $|\xi_B\sigma| < 1$, $|\xi_R\sigma| < 1$. All are simpler written in terms of λ, R_ρ. The values of λ, R_ρ appearing in Eq. 1.50 have to be self-consistent solutions of the original cubic equation for R^2. In the following examples, we shall form the self-consistent values by using the parametrization introduced in section 1.2.7, and scanning a. Better still is to perform the scan in bandwidths of the resonator, using

the variable $b \equiv a/\epsilon$. When b (or a) is used as the independent variable, the resonance is unfolded: the tilt of the amplitude curve R_ρ is removed, and the frequency $\lambda(b)$ is not monotonic increasing.

Curve B slavishly follows R. Curve A follows R everywhere except $b = 0$, where A has a zero. Figures 1.8 and 1.9 show values for the hard and softening oscillators in the regimes: (1) R_ρ is single valued, and (2) triple-valued. When R_ρ is single-valued, Fig. 1.8, the values ξ_B and ξ_R can be tamed with a slew rate $|\sigma| = 1\%$. When R_ρ is triple-valued, Fig. 1.9, it is clear that no matter how small we make the slew rate σ (provided it is not zero) the conditions are violated, the singularities can be tamed, and there will be a jump.

1.4.1 Explanation

The curve B'/B is so very similar to $(R^2)'/(R^2)$, that there is no need to plot both curves. The curve A'/A is quite distinct because A has a zero at $\lambda = R_\rho/2$, as may be seen from Eq. 1.7. [At the same $\lambda = R_\rho/2$, B is almost a maximum.] Hence this singularity $A'/A \to \infty$ is bogus. Linear instability is seeded by the difference in states between $\sigma = 0$ and $\sigma \neq 0$. When R_ρ is triple-valued, amplitude growth is launched by the linear instability that ensues at λ_s (jump-down) or λ_t (jump-up); the nonlinear mechanism rapidly assists and takes over leading to run-away; the instability ends in a new state (on the opposite branch) where the linear damping is restored. When R_ρ is single-valued, there is damping at either side of the interval λ_s to λ_t; it does not matter whether the SS amplitude is smaller or larger than the values in the interval; it only matters that λ is outside the interval. Thus, when amplitude growth is launched by the linear instability (flinch) that occurs between λ_s and λ_t; the nonlinear mechanism takes over and rapidly damps the nascent instability.

1.4.2 Latching

The curve ξ_R is a proxy for ξ_A and ξ_B. Figure 1.10 shows the curves $\xi_R(b)$ along with $R_\rho(b)$ and $\lambda(b)$. The latter two (not to scale) guide the eye as to the range of b values where R_ρ is triple valued. Wherein tripled valued, the resonance curve is shown red (otherwise blue) and the drive frequency λ (shown in coral) has a local dip or bump. The curves of ξ_R are colour coded according to whether there is a jump-up (light green) or jump-down (dark green).

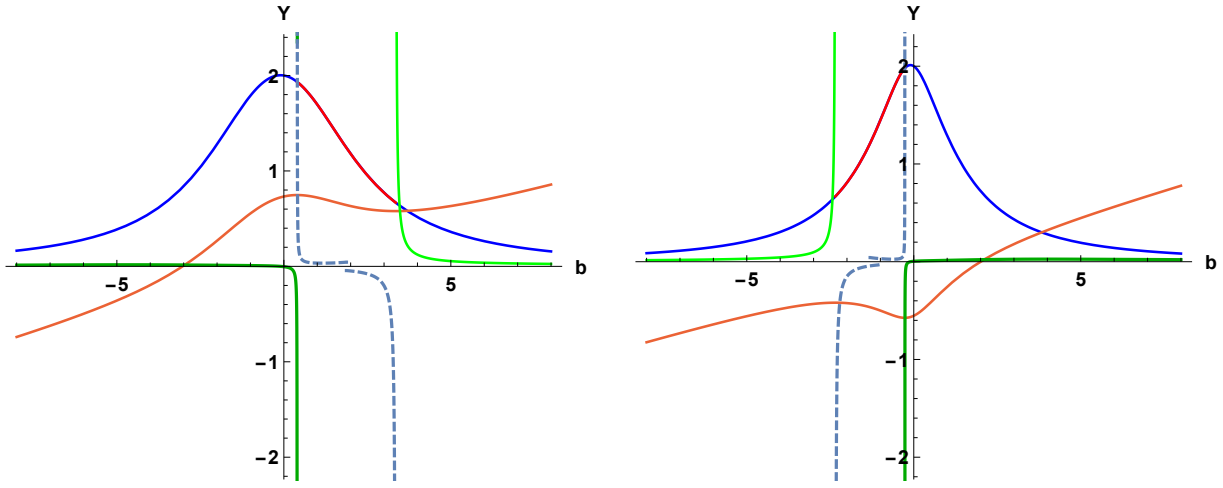

Figure 1.10: Plot of the normalised derivative $Y \equiv (R^2)'/(R^2)/(5000\epsilon\sigma)$, shown green and gun-blue versus b. Superposed is resonance curve (shown blue and red); and $2 \times \lambda(b)$ shown to scale (colour coral). Left: hardening resonator ($\epsilon = 0.1, \rho = +0.01$). Right: softening resonator ($\epsilon = 0.1, \rho = -0.004$).

The resonance has been unfolded; actually it folds back on itself in the red zone. Figure 1.10

left: jump down near $b = 0$ (occurs at higher frequency) shown dark green; jump up on the far right (occurs at lower frequency) shown light green; signs are reversed on the right because frequency sweep is descending. "To the other side of the poles" (shown gun-blue) is inoperative due to the jump. Figure 1.10 right: jump up on the far left (occurs at higher frequency) shown light green; jump down near $b = 0$ (occurs at lower frequency) shown dark green; signs are reversed on the right of each plot because frequency sweep is descending. Inoperative part of the poles is shown dashed gun-blue; inoperative because after the jump the former pole lies on the opposite branch.

1.4.3 Continuous derivative

Figure 1.11 shows the curve $\xi_R(b)$ (scaled) along with $R_\rho(b)$ and $\lambda(b)$ when the resonance curve is single valued. The curve ξ_R is for $\sigma > 0$, and would be reversed in polarity for a down-sweep $\sigma < 0$. It is clear that $|\xi_R|$ can be held below or around unity if the slew is $|\sigma| = 1\%$ or less. Moreover, if we imagine integrating R' to obtain the resonance curve, it evident that the integral rises smoothly to a maximum and then descends due to the sign change that occurs at $b = -\epsilon$.

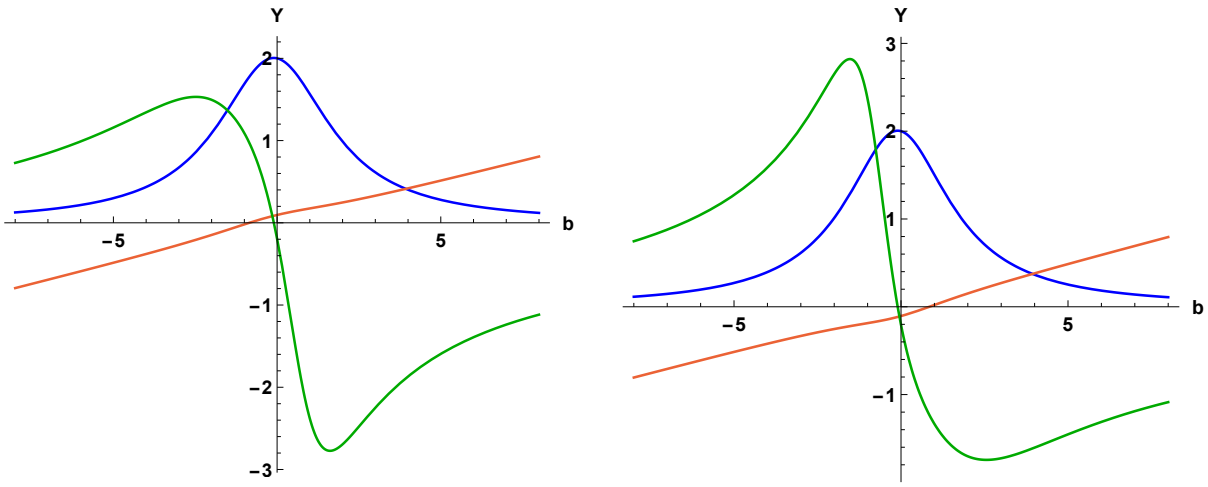

Figure 1.11: Plot of the normalised derivative $Y \equiv (R^2)'/(R^2)/(100\epsilon\sigma)$, shown green versus b. Superposed is the single-valued resonance curve (shown blue); and $2 \times \lambda(b)$ shown to scale (colour coral). Left: hardening resonator ($\epsilon = 0.1, \rho = +0.001$). Right: softening resonator ($\epsilon = 0.1, \rho = -0.001$).

1.4.4 Jump mechanism

Although we cannot pin down the minute details of the mechanism, we can clearly see that as soon as ξ_A or ξ_B are significant (comparable with $1/\sigma$) then the equilibrium will collapse in a run-away effect. We may state the mechanism qualitatively. The resonance curve is shaped by the competition between drive and dissipation. At the lower/upper TP, disturbance of the equilibrium reveals there is an excess of drive/dissipation that propels the system toward a new equilibrium on the opposite branch. For the hardening MSO, lower branch, down sweep: the amplitude starts to rise, then the resonance frequency starts to rise toward the falling drive frequency, and the amplitude increases even faster giving a positive feedback loop. The resonance frequency is pulled toward the drive frequency in a run-away. On the upper branch, with an up sweep: amplitude starts to fall, then the resonance frequency starts to fall while the drive frequency continues to rise, and the amplitude falls even faster; drive (and particularly) the resonance frequency move away from one another, and the amplitude collapses.

In short: in the *sweep down, jump-up*, the resonance frequency is "pulled" up toward the (falling) drive frequency; in the *sweep-up, jump-down*, the resonance frequency is "pushed" down away from the (rising) drive. For the softening resonator, the situation is reversed: in the *sweep-up, jump-up*, the resonance frequency is "pulled" down toward the rising drive frequency; in the *sweep-down, jump-down*, the resonance frequency is "pushed" up away from the falling drive. This suggests a phenomenological model of the jump based on the Green's function for the SHO in which the resonance frequency is made time-dependent: $\alpha(t)$ moving toward the jump-up frequency or away from the jump-down frequency.

1.5 Jump Phenomena

1.5.1 Jump preceded by linear instability

Many authors[10, 11, 12, 15, 23] do not make any distinction between the linear-instability points and the tuning points, assuming that since they differ by order ϵ^2 there can be no material difference. They conflate the upper stability point $(\lambda_s, R_{\rho\, s})$ with the maximum $(\lambda_r, \hat{R}_\rho)$. [They replace Eq. 1.23 by Eq. 1.24, and the limiting value of $\rho < 0$ Eq. 1.22 by simply $-\epsilon^2/2 < \rho$.] This leads to the assertion that perturbations on the lower and upper branches are stable, and that only system states on the middle branch are unstable with respect to small perturbations. This, in turn, leads to the perplexing (and mistaken) result that there is a jump instability despite the fact that the resonator state is never on the middle branch. But it is crucial to make the distinction between the instability points and the turning points. It is noteworthy that Jordan[23] Chap. 7.3 insists that only the middle branch is linear unstable, but shows in his Fig. 7.8 numerical solutions of the EOM whose "run-away" point of departure coincides with the linear-instability points derived herein. Contrastingly, Magnus[3] retains terms in ϵ^2 and gives the exact expression for the maximum, Eq. 1.23. Magnus also makes the distinction between the maximum and the TP, but does not give an expression for the latter. Brennan[15] makes the approximations that (i) the jump-down location is the resonance maximum, and (ii) the jump-up location is that of the resonance envelope when $\delta = 0$. Howver, it is more important to have accurate values than simple formulae.

Jumps occur only when R_ρ is triple-valued. The jump takes place during the frequency sweep from the location of the instability threshold to that of the nearest turning point. The jump starts as a conventional linear instability, but quickly departs into the nonlinear regime. As the oscillation enters this regime, the terms $\dot{A}, \ddot{A}, \dot{B}, \ddot{B}$ become overwhelmingly the dominant terms in the equation of motion; and indeed the EOM becomes Eqs. 1.48 and 1.49. After the impulse, the amplitude settles on a different branch at which location small deviations are again damped. There is no need to invoke an external noise source as the cause of the initial small perturbation as the system enters the jump zone, because there are always deviations present between the dynamic steady state (occurring in the sweep) and the absolute steady state (of a fixed frequency excitation).

When R_ρ is single-valued, a resonator state that lies on or passes through the narrow linear instability band $(\lambda_s < \lambda < \lambda_t)$ is momentarily unstable. However, the condition is self-stabilizing: any change in the resonator amplitude (either increase or decrease) moves the state into the λ range where there is damping. Hence, a non-linear mechanism suppresses the instability. The resonator stays on the single resonance curve, and the positive and negative values of A' about the singularity cancel as the drive frequency is swept. It does not matter whether the sweep is up or down, because the system is more stable at either side (above or below) the instability band.

1.5.2 The Flinch

The rapid transition between the stable states of a bi-stable resonator is called a jump. A name is needed for a momentary instability in a single-state resonator that is rapidly suppressed. The effect is so small that it does not warrant the term "hop". We propose "flinch" which has (among

several) the dictionary defined meanings: shrink from, turn aside, wince (shrink away involuntarily). A flinch-alone occurs only when R_ρ is single-valued.

When R_ρ is triple-valued, the flinch launches the jump. When R_ρ is single-valued, the flinch is present but inconsequential. The width of the resonance, measured in units of $w = \omega/\sqrt{\alpha}$ is roughly 4ϵ; measured in units of λ it s about 8ϵ. The width of the flinch is order $\epsilon/4$. Hence, as ϵ decreases, the flinch becomes increasingly difficult to resolve graphically in resonance plots and to observe experimentally. This does not mean the flinch disappears; it continues an essential ingredient in the jump scenario; but it is easily missed in an experimental environment.

When R_ρ is single-valued, the separations between $\lambda_r, \lambda_s, \lambda_t$ is of order ϵ^2. When R_ρ is multi-valued, the separations between $\lambda_r, \lambda_s, \lambda_u$ and the separation between λ_l, λ_t are of order ϵ^2. Hence analytical results that do not resolve frequency difference of ϵ^2 may not distinguish between the turning points and linear-instability points. But conflating them leads to mistaken conclusions.

1.5.3 Jump landscape

The jump requires a nonlinear mechanism. This may be understood in terms of the landscape of poles and zeros of the derivative dR/dw. This insight precedes the details of Sec. 1.4. The cubic equation for R^2, or R_ρ, has three branches. Likewise, the derivative $dR^2/dw = 2R \times dR/dw$ has three branches. The branches join where $d\lambda/dR_\rho = 0$. These locations are singularities (poles) of dR/dw. Imagine that we try to find R by integrating dR/dw. At the branch frequency λ_l closer to $\lambda = 0$, there are two small and one large solution R. If we insist R is continuous, then we follow from one small solution to the other; from the lower branch to the middle branch. In this case, the negative and positive impulses[10] of dR/dw (around the singularity) cancel in the manner of a principal value integral. However, it is legitimate to jump to the upper branch. In this case, there is no canceling impulse in dR/dw; and the upward impulse in dR/dw is sufficient to generate the jump-up.

Similarly, at the branch frequency λ_u further from $\lambda = 0$, there are two large and one small solution. If we insist R is continuous, then we follow R from the upper branch to the middle branch. In this case, the negative and positive impulses of dR/dw (across the singularity) cancel. However, because dR/dw is indeterminate at the singularity, it is legitimate to jump to the lower branch and continue to evaluate dR/dw. In such a case, there is no canceling impulse; and the downward impulse in dR/dw is sufficient to generate the jump-down.

In the case of the physical oscillator, rather than the mathematical abstraction, the oscillator always jumps. As the drive frequency is swept in the neighbourhood of a branch frequency, the oscillator receives a first impulse and jumps to the opposite branch where the SS conditions are so different that there is no second impulse to cancel the effect of the first. Now, $dR/dz = (dR/dw)(dw/dz) = (dR/dw)\sigma$ and so the sign of the impulse is directly influenced by that of σ, and that is the cause of a latching effect. For the hardening oscillator, the down-sweep results in a jump-up and the up-sweep results in a jump-down. For the softening oscillator, the latching leads to sweep-up and jump-up, or sweep-down and jump-down. The latching effect is indicated in Fig. 1.10.

1.5.4 Comparison with dual scales

There already exists a mathematical analysis of the jump phenomena[5, 6, 10, 11, 12]. The key step is to introduce two time scales, fast and slow. We give an account of it in Appendix C. It is elaborate and approximate and involves sleight of hand. It attempts to give a description of *all the dynamics*, and oscillator states, thay may occur across a wide range of drive frequency. But it is not the intention to find accurate formulae for maxima or turning points. In broad strokes,

[10] Technically an impulse is a brief and powerful force that effects a discontinuous change in velocity. Here, analogously, the "impulse" results in a discontinuous change of amplitude.

the second derivatives $\ddot{A}, \ddot{B}$ are discarded and a system of nonlinear evolution equations for $\dot{A}, \dot{B}$ are developed. These equations may be derived from a Hamiltonian structure in the limit that dissipation goes to zero ($\delta \to 0$). A is given the role of position, and B the associated conjugate momentum. There is no physical implication in this; it is purely artifice that enables us to use the Hamiltonian machinery, in particular phase space, to examine the motion without finding explicit solutions for the time dependence of either $A(t)$ or $B(t)$. [From the outset, the decision to discard $\ddot{A}, \ddot{B}$ was informed by the desire and goal of obtaining a Hamiltonian-like system.] When dissipation is restored, the phase space trajectories are perturbed: either drawn toward attractors (stable fixed points) or repelled from saddle points. The locations of the fixed points of motion also move when dissipation is restored ($\delta \neq 0$). Certainly the analysis generates jump phenomena; but we might even say *too many* of them. There is a range of parameter values over which there are jumps possible between all three branches. The very fine-structured nature of bifurcations can make it difficult to state precisely from where a jump commenced. This imprecision and non-localisation of the jumps is a consequence of discarding the second derivatives. Higher derivatives are associated with sharpness of rise or fall, as is obvious when a function is expanded as a Maclaurin or Taylor series.

In contrast, we have focused on a description of specifically and exclusively the narrow ranges of frequency within which the jump-up and jump-down are believed to occur based on analysis of the turning points when dissipation is included. This description relies on all of the derivatives being sufficiently large that they dominate the EOM to the extent that steady state terms may be discarded.

1.6 Numerical Examples

In this section we shall use numerical integration of the EOM to investigate the behaviour of the MSO for a range of parameters wherein the resonance may be single- or triple-valued function of the excitation frequency which is swept. The numerical solution immediately runs into a difficulty: whereas analytically it is easy to form the mean square value of the oscillation $\langle x^2(t)\rangle$, this is not so for numerics because it requires an averaging over the previous history of the oscillator. One would have to contemplate a procedure in which we keep a moving window record of the motion during the previous period, and compute the means square value within the window to give the present value. The record could be a First In First Out (FIFO) register, initially filled with equal values. However, we do not attempt such a complicated procedure. Instead we simply compute the following estimate:

$$\langle y^2\rangle \;\approx\; \left\{y(z)^2 + [y'(z)/w(z)]^2\right\} \quad \text{and} \quad w = w_0 + \sigma z\ . \tag{1.51}$$

For the up-sweep, starting from near DC we use the initial values $y(0) = 1, y' = 0$. For the down sweep, starting from a frequency distant (i.e. well above) from resonance, we use the initial values $y(0) = 0, y' = 0$. Thse conditions are not perfectly matched to the steady-state values.

1.6.1 Resonance curves

In the main sequence of examples, the nonlinearity metric ρ is held constant and small while the damping rate ϵ is varied in the weak regime. In addition a variety of sweep rates $|\sigma| = \epsilon/N$ with $N = 400, 800, 1600$ was used to find if there is sensitvity to the slew. In each case the numerically computed up-sweep is shown blue and the down-sweep in red. The theoretical resonance curve for $\sigma = 0$ is shown in green-dashed. There are additional examples in Sec. A. In particular, Fig. A.4, a case with much larger $|\rho|$ and ϵ chosen large enough for a (mostly) stable response curve.

Fig. 1.12 shows the single-valued response curve for hard and soft resonators that arises when the damping rate is sufficiently large ($\epsilon = 0.1$). The numeric and analytic resonance curves are very similar. Further, there is little difference whether $N = 400$ or 800 is used.

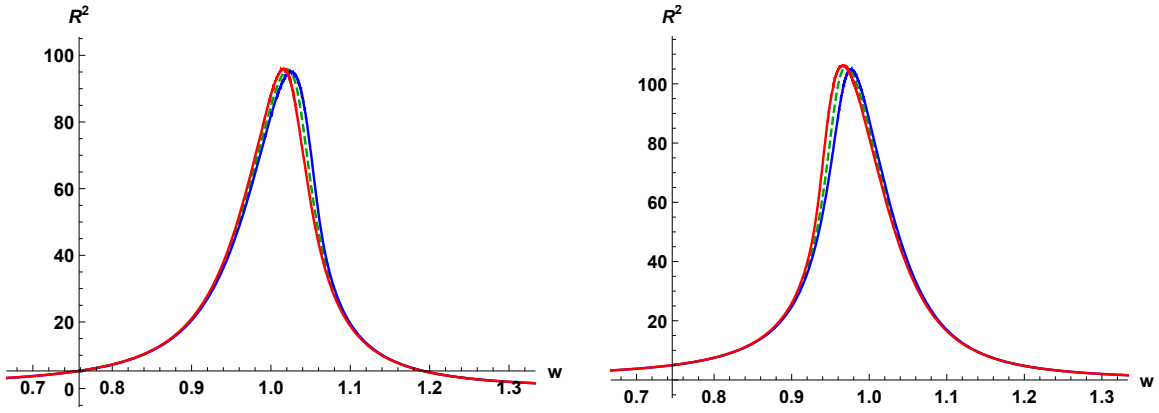

Figure 1.12: Swept frequency response with $\epsilon = 0.1$, $\rho = \pm 0.001$, $|\sigma| = \epsilon/800$. Blue curve = up-sweep. Red curve = down-sweep. Left: hardening oscillator. Right softening resonator.

Fig. 1.13 shows the triple-valued resonance that emerges when the damping rate is reduced to $\epsilon = 0.05$. The up- and down-jumps are clearly visible, and occur at the frequency of the turning points of the analytic response curve. There are overshoots followed by small transient oscillations after the jump; and these are slightly more pronounced when the slew rate is increased from $|\sigma| = \epsilon/800$ to $|\sigma| = \epsilon/400$.

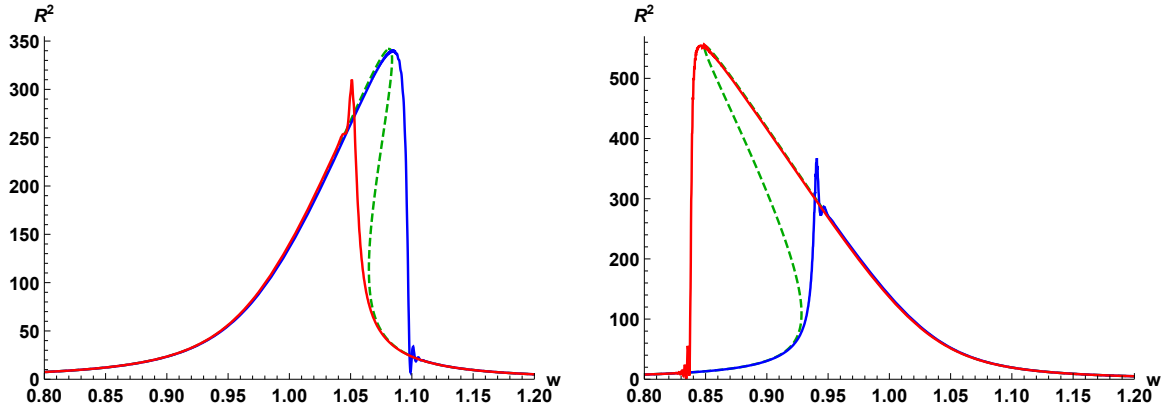

Figure 1.13: Swept frequency response with $\epsilon = 0.05$, $\rho = \pm 0.001$, $\sigma = \epsilon/800$. Left: hardening resonator. Right: softening resonator. Blue curve = up-sweep. Red curve = down sweep. Green-dashed curve = theoretical resonance curve when $\sigma = 0$.

Fig. 1.14 shows the strong nonlinear regime that arrises when the damping rate is further reduced to $\epsilon = 0.01$. For each resonator type (hard or soft), the up- and down-sweeps are vastly different. The jump frequencies continue to be pedicted by the turning points of the analytic response curve. In the case of the softening resonator, the nonlinearity metric was reduced to $\rho = -0.00004$ which is above the instability threshold $\rho = -0.00005$. There are no steady-state solutions of the EOM for negative detuning when ρ is more negative than the threshold value. Again, there is overshoot and transients after the jumps; particularly evident for the jump-up.

1.6.2 Flinch instability

At the resolution of the graphs, Figs. 1.12–1.14, the resonance curves appear to have no fine structure except at the jumps. However, if we zoom-in we find small-amplitude high-frequency ripple in the neighbourhood of the maximum for the single-valued resonance, and in the neighbourhood

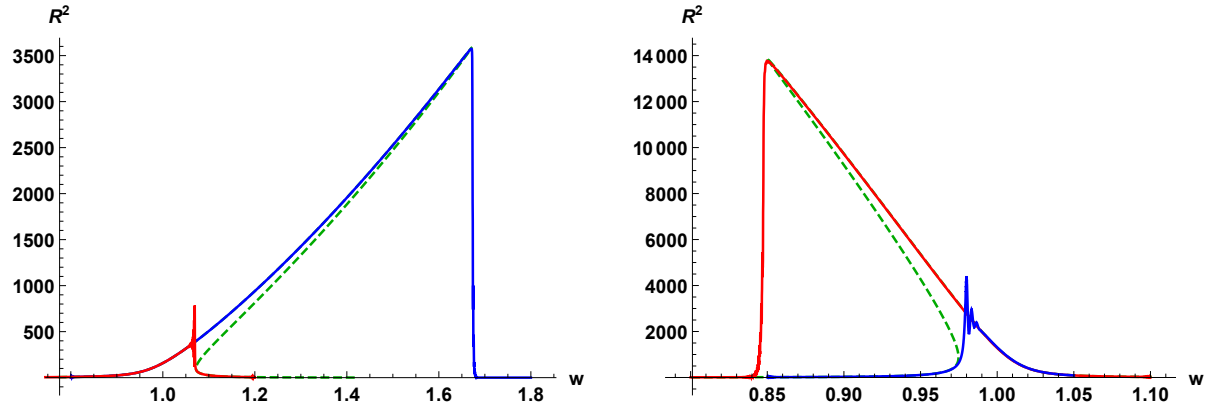

Figure 1.14: Swept frequency response with $\epsilon = 0.01$ and $|\sigma| = \epsilon/800$. Left: hardening resonator with $\rho = +0.001$. Right: softening resonator with $\rho = -0.00004$.

of the turning points (prior to the jumps) for the triple-valued resonance. Although this ripple could be seeded by inexact initial matching conditions, or arise from the frequency sweeping, we propose that the ripple is attributable to the flinch instability. The amplitude of the fine structure diminishes as the slew is reduced from $|\sigma| = \epsilon/400$ to $|\sigma| = \epsilon/1600$ but does not disappear. To make the flinch instability more apparent, we have plotted sweep simulations with $|\sigma| = \epsilon/400$.

There is ample evidence in Figs. 1.15 and A.5, A.7 of the flinch occurring when the resonance is single-valued. During the frequency sweep, an oscillation emerges in the region of the maximum and decays to either side. It should be noted that in this region, R_ρ is slowly changing, so dynamical effects (of for example sweeping) should be the least pronounced.

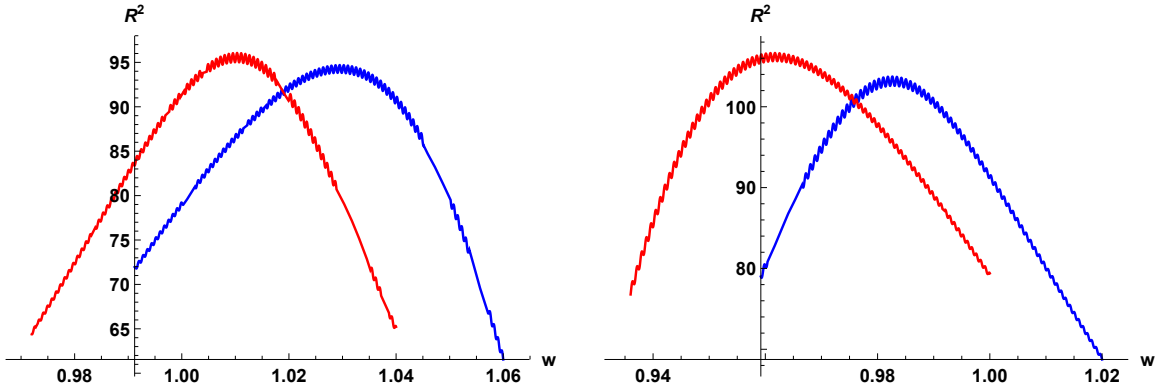

Figure 1.15: Frequency sweep in vicinity of maximum with $\epsilon = 0.1$ $|\rho| = 0.001$. Blue curve = up-sweep. Red curve = down-sweep. Left: hardening resonator. Right: softening resonator.

There is also evidence of a flinch prior to the jumps in Figs. 1.16 and 1.17 when the resonance is triple-valued for both the hardening and softening resonator when $\epsilon = 0.05$. Fig. 1.16 is the counterpart of Fig. 1.13-Left; and Fig. 1.17 is the companion of Fig. 1.13-Right.

However, when the damping rate is reduced to $\epsilon = 0.01$, the precursor flinch is less clear. In Figs. 1.18 and 1.19, flinch oscillations begin before the jump-down for both hard and soft resonators. But there is no evidence of a flinch instability occuring prior to the jump-ups. There are obvious overshoots and transients following the jump-ups. This is certainly a mystery. The mystery is reinforced in Fig. A.6 for the hardening resonator with strong nonlinearity. Fig. 1.18 is the counterpart of Fig. 1.14-Left; and Fig. 1.19 is the companion of Fig. 1.14-Right.

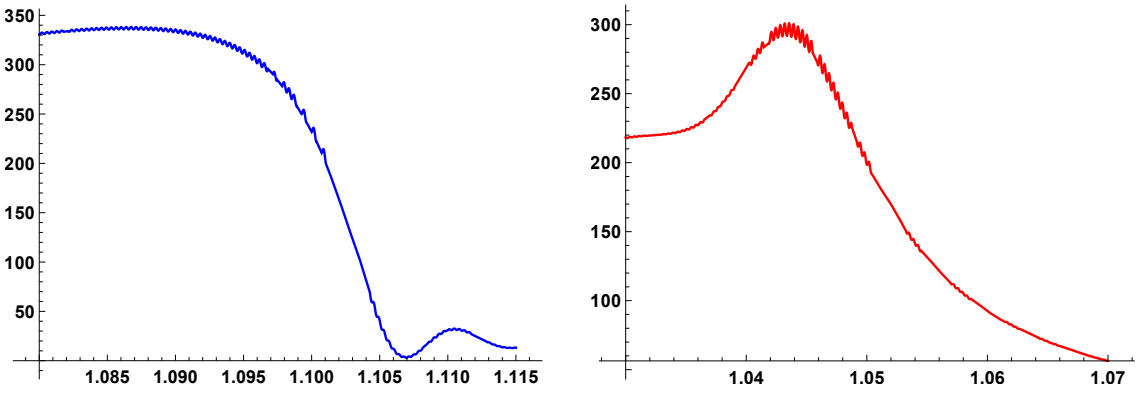

Figure 1.16: Hardening resonator: $\epsilon = 0.05$ $\rho = +0.001$. Left: up-sweep, jump-down . Right: down-sweep, jump-up.

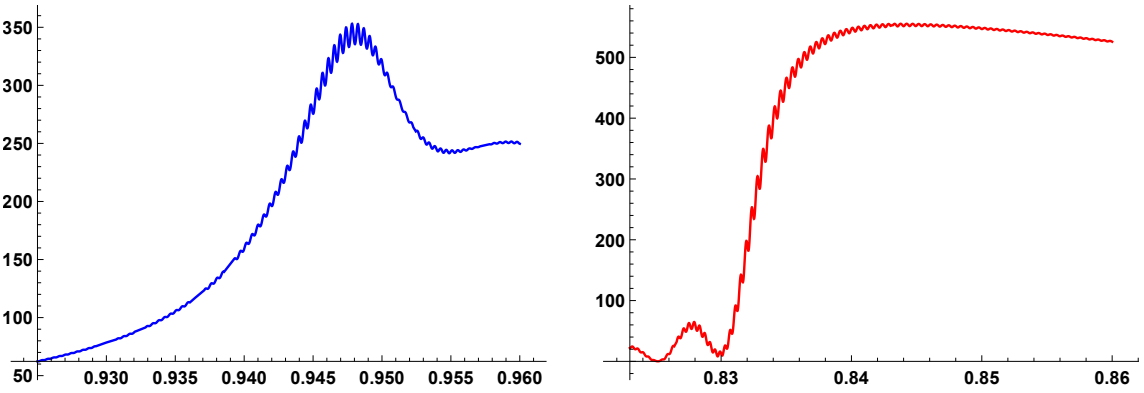

Figure 1.17: Softening resonator: $\epsilon = 0.05$ $\rho = -0.001$. Left: up-sweep, jump-up. Right: down-sweep, jump-down.

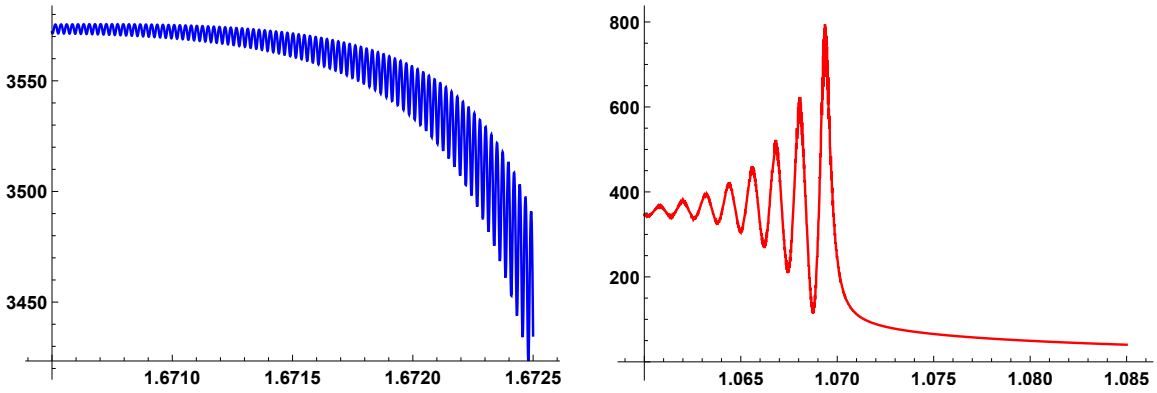

Figure 1.18: Hardening resonator: $\epsilon = 0.01$ $\rho = +0.001$. Left: up-sweep, jump-down. Right: down-sweep, jump-up.

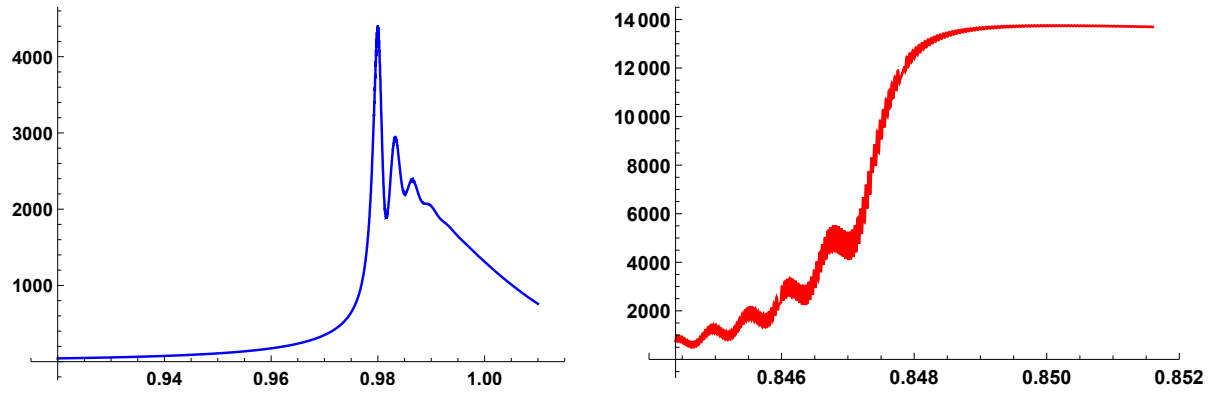

Figure 1.19: Softening resonator: $\epsilon = 0.01$ $\rho = -0.00004$.Left: up-sweep, jump-up. Right: down-sweep, jump-down.

1.7 Origin of the Mean-Square Oscillator

The MSO arises from two ingredients: (1) the restoring force has a cubic terms $\beta x(t)^3$, and (2) there is a filter that attenuates harmonics of the fundamental. Examples of such a filter are another linear, narrow-band resonator or a passive element G with a long time constant. The MSO equation of motion is Eq. 1.3. The Duffing EOM replaces $\langle x^2 \rangle$ by $x(t)^2$. Let $\tau = 2\pi/\omega$ be the drive period. The mean-square value is

$$\langle x^2 \rangle = \frac{1}{\tau} \int_{-\tau/2}^{+\tau/2} x(r) G(t-r) dr \ , \tag{1.52}$$

where the kernel $G(t)$ is a response function, and the bra-kets denote a time average performed over one or more cycles. For example, G may be the relaxation $G(t) = \exp(-t/T)$ or the instantaneous response given by the Dirac delta function. Suppose the response to the external sinusoidal drive is $x(t) = a\cos\omega t + b\sin\omega t$, and calculate the average $\langle x(t)^2 \rangle$ for two cases. For brevity, let $z \equiv \omega T$ and $\hat{x} > 0$ be the oscillation amplitude. The relaxed case:

$$\begin{aligned}
\langle x(t)^2 \rangle &= \frac{1}{\tau} \int_{-\tau/2}^{+\tau/2} (a\cos\omega r + b\sin\omega r)^2 \exp[(r-t)/T] dr \\
&= \frac{z\exp(-t/T)\sinh(\pi/z)}{\pi(1+4z^2)} [a^2 - 2abz + 2(a^2+b^2)z^2] \\
&\approx \frac{1}{2}(a^2+b^2)\left[1 - \frac{1}{12}\left(\frac{\tau}{T}\right)^2\right] - \frac{ab}{4\pi}\left(\frac{\tau}{T}\right) \quad \to \quad \frac{1}{2}(a^2+b^2) = \frac{1}{2}(\hat{x})^2 \quad \text{for } T \gg \tau \ .
\end{aligned}$$

Thus arises the MSO. Alternatively, the case of instantaneous response:

$$\langle x(t)^2 \rangle = \frac{1}{\tau} \int_{-\tau/2}^{+\tau/2} (a\cos\omega r + b\sin\omega r)^2 \delta(r-t) dr \ = \ x(t)^2 \ . \tag{1.53}$$

recovers the Duffing oscillator with the cubic term $\beta\, x(t)^3$. Despite apparent similarity, the DO and MSO are fundamentally different in one respect. The DO cubic term produces frequency multiplication, also sum and difference frequencies. There is no such response for the MSO because $(\hat{x})^2$ does not contain frequency components. Small amplitude excitation of the DO at one third the resonance frequency will produce large amplitude response at the resonance frequency because $\cos(z)^3 = [3\cos z + \cos 3z]/4$. The exact steady-state amplitude response of the DO to a sinusoidal drive is *unknown*! In principle, it contains an infinite number of harmonics of the drive, all of different amplitude. Truncated approximate forms have been obtained using computer algebra, but are mathematically fragile. Contrastingly, the amplitude response of the MSO is known; and it contains only one frequency component.

1.7.1 Two examples of mean-square resonators

Both examples are drawn from the realm of metallic cavity resonators that contain electro-magnetic (EM) fields oscillating at radio-frequency (typically in the MHz to GHz range). The first example is a normal-conducting (copper) cavity with a ferrite-loaded region to reduce the cavity length. Actually, the first example is a *candidate* rather than defnitely a mean-square oscillator. The physical properties of ferrites are various and complicated, as are the explanations of those properties. Ferrites are intrinsically (but weakly) nonlinear with respect to RF amplitude, and have more than one relaxation time scale. The ferrite properties are varied by an applied quasi-DC magnetic field, called a biasing field. The resonance frequency is tuned by altering the bias. There are two types: (1) parallel bias of nickel-zinc ferrite, and (2) perpendicular bias of (rare earth) garnet ferrite. The orientation of the bias is relative to the RF magnetic field component. Although both types employ ferrites, the physics of each is very different. In the conventional type (1) the ferrite is lossy and contributes to damping of the oscillations; and a single-valued resonance curve is observed at high power levels; Moreover, the allowable level of dissipation is limited by cooling; and the input power cannot be further raised to levels that might expose nonlinear behavior. In the less common type (2) the material is operated above the ferri-magnetic resonance leading to high magnetic and electric quality factors. In protoype[24] cavities with low-loss yttrium-garnet ferrites, the RF magnetic field can be so large that it contributes to the biasing field. It appears that the mean-square value of the RF field that alters the bias. Experimental observations[25], with swept frequency excitation at different power levels, are consistent with the properties of a hardening oscillator. Theoretical anlaysis by Shapiro[26] also shows the orthogonal-biased ferrite to have the properties of a hardening oscillator. The only way to be sure this is a MSO rather than DSO would be either (i) to excite at the 1/3 sub-harmonic and measure the response at the fundamental; or (i) excite at the fundamental and measure a response at the 3rd harmonic. Both measurements are difficult because the quality factor is several thousand, and so the response signals would be very small.

The second example is the so-called "ponderomotive effect" in metallic cavities operated at high EM-field strength. Technically, it is not the ponderomotive force which specifically arises in a non-uniform EM field; but the name has stuck. Rather it is the Lorentz force due to the interaction of the surface magnetic field with the surface current, and surface electric field with the surface charge, on the interior surfaces of the cavity. The interior pressure is $P = \mu_0 H^2 - \epsilon_0 E^2$, where $\mu_0\epsilon_0$ are the permeability and permittivity and E, H are the electric and magnetic fields, respectively. The effect is particularly pronounced in superconducting cavities fabricated from niobium and cooled to 4 Kelvin or below by liquid helium. These cavities are almost lossless, with quality factor in the range $Q \simeq 10^9$ or higher. So strong are the electromagnetic fields that can be sustained in these cavities that the Lorentz force arising on the interior surface of the cavities is strong enough to mechanically deform[27] the cavity walls. To be clear, it is the mean-square value of the RF field that acts on the walls. The walls deform, and the nett effect is for the resonance frequency to fall - in the manner of a softening resonator. These cavities are widely used in charged-particle accelerators, and have an extensive literature[28, 29]. However, the precise nature of the non-linear resonator is not studied in that literature.

Let the phase of the EM-field be $z = \omega t$. Given that the cavity eigen-frequency is related to the cavity dimensions, and that the EM field attempts to deflect the cavity surface proportional to $H^2(z)^2 = \frac{1}{2}H^2(1+\cos 2z)$ and there is a putative nonlinear term $\Delta\alpha \times H(t) \propto H^3(1+\cos 2z)\cos z \propto \frac{1}{2}H^3(3\cos z + \cos 3z)$, why is this second example *not* a Duffing oscillator? The metal is a conduction band of dissociated electrons (electron sea) in a lattice of massive anions (atomic nucelus plus inner shell electrons). The electrons do respond to the Lorentz pressure, but the nuclei are of order 10^5 times more massive. Moreover, for the metallic surface to significantly deform requires the cooperative movement of order 10^{18} nuceli. Thus due to inertia and stiffness, the metallic walls respond on a time-scale of kHz. Hence the nonlinear term is $\Delta\alpha \times H(t) \propto \langle H^2 \rangle H(t)\cos z$ where the mean-square average is formed over thousands (or millions) of MHz (or GHz) RF cycles.

1.8 Conclusions

The following are new: the mean-square oscillator and its properties; the dynamic equilibrium state in a swept frequency system; the emphasis on and use of self-consistency; the explicit thresh-old ρ for emergence of the triple-valued regime; proof that linear instability extends beyond the middle branch and that a threshold exists even when R_ρ is single-valued; discovery of the "flinch" phenomenon when R_ρ is single-valued; a predictive explanation of jump phenomena based on the poles and zeros of dR^2/dw (the derivative of steady-state amplitude response with respect to drive frequency). The last is a powerful insight, and likely applies to nonlinear resonators in general. Our analysis extends from the weak to critically damped ($\epsilon < 2$), and from the weak to strong nonlinear regime of hardening and softening resonators. The numerical simulations confirm the existence of the flinch in some cases, but leave a puzzle: no obvious flinch signature prior to the jump-up for weakly damped resonators.

We have compared and emphasised two distinct regimes: the statics-dominated regime, in which the constant terms in the EOM dominate and the derivatives are discarded; and the dynamics-dominated regime, in which the derivative terms in the EOM dominate and the constant terms are discarded. This leads in a natural way to the jump phenomena: rather than being unexpected they become inevitable and inescapable. The two regimes of approximation each have a different equation of motion. Away from the jump zones, the EOM is essentially Eqs. 1.7, 1.8. Contrastingly in the jump zones, the EOM becomes Eqs. 1.48, 1.49.

We mention here a possible direction for future work. In the jump explanation recounted in Sec. C, the use of dual time scales and the approximation to Hamiltonian mechanics are both essential components. However, the decomposition into zeroth and first order appears dispendable. Therefore, it would be interesting to investigate if the same methods can be applied directly to the harmonic balance equations Eq. 1.5 and 1.6.

1.8.1 Relation to the Duffing oscillator

In the regime of particular interest, the jump phenomena, the resonator is weakly damped and sufficiently narrowband that the resonance is clearly triple-valued. In the case that motion is dominated by the fundamental resonance, the Duffing resonator shares exactly the same system equations, for the description of its steady state and for the stability analysis of small perturbations, as the mean-square oscillator. Hence the analysis and elucidation of the jump mechanism applies equal well to the Duffing resonator. When the oscillator is so very broadband that many harmonics are significant, the oscillations are very over-damped; and nonlinear instability is extremely unlikely.

Appendix A

Additional Examples

A.1 Analytic frequency sweeps

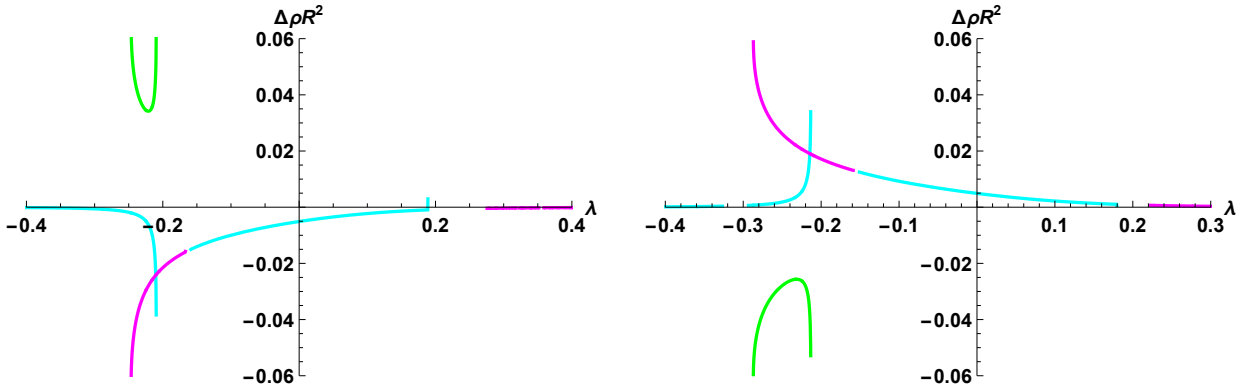

Figure A.1: Hardening resonator difference curves $R_\rho(\lambda, \sigma \neq 0) - R_\rho(\lambda, \sigma = 0)$ for $(\epsilon = 0.1, \rho = +0.04)$ and $\sigma = 0$ or $|\sigma| = 0.01$. The cyan, magenta and green segments map to the solutions x_1, x_2, x_3 respectively. Left: Frequency up-sweep $\sigma > 0$. Right: Frequency down-sweep $\sigma < 0$.

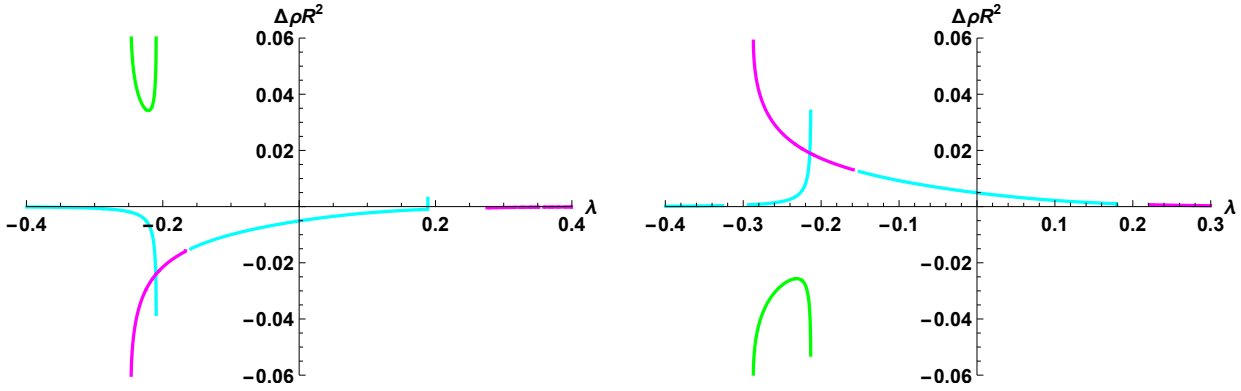

Figure A.2: Softening resonator difference curves $R_\rho(\lambda, \sigma \neq 0) - R_\rho(\lambda, \sigma = 0)$ $(\epsilon = 0.1, \rho = -0.004)$ and $\sigma = 0$ or $|\sigma| = 0.005$. The cyan, magenta and green segments map to the solutions x_1, x_2, x_3 respectively. Left: Frequency up-sweep $\sigma > 0$. Right: Frequency down-sweep $\sigma < 0$.

A.2 Numerical frequency sweeps

Figure A.3 is a counterpart to Fig. 1.13 which shares the same damping rate. Here the modulus of nonlinearity parameter ρ has been reduced in order to restore a single-valued resonance curve.

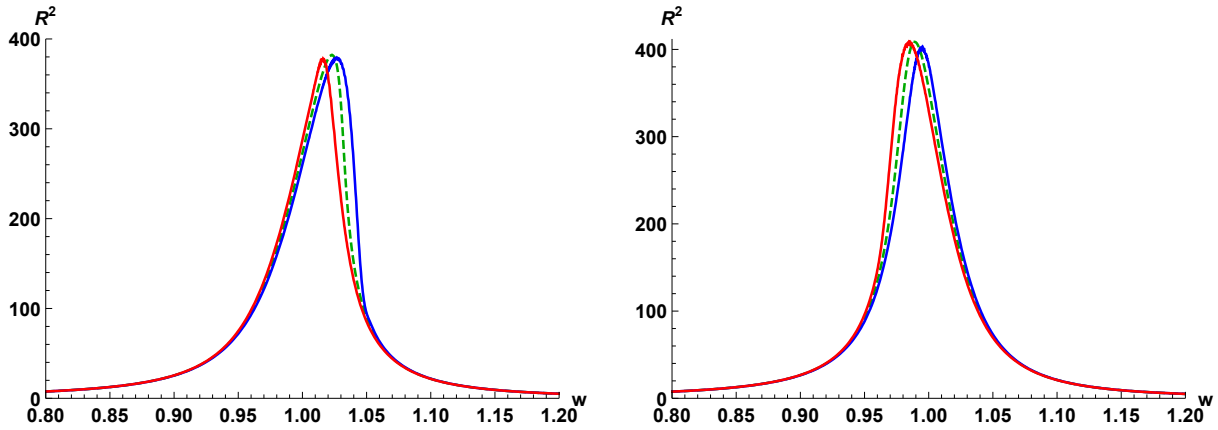

Figure A.3: Swept frequency response with $\epsilon = 0.05$ and $|\sigma| = \epsilon/800$. Blue curve = up-sweep. Red curve = down-sweep. Green-dashed = theoretical response whne $\sigma = 0$. Left: hardening resonator, $\rho = +0.00025$ Right: softening resonator, $\rho = -0.0001$.

Figure A.4 shows response curves for large nonlinearity parameter ρ. The left figure shows the triple-valued resonance of a hardening oscillator with jump phenomena located at the turning points of the theoretical response curve. The right hand figure is for a softening resonator. The damping rate was increased ($\epsilon = 0.8$) to achieve a steady state below the nominal resonance frequency. The situation is fragile: there is an obvious transient at the beginning of the up-sweep. Moreover, if ρ is made more negative ($\rho = -0.225$) the down sweep ends in a run-away.

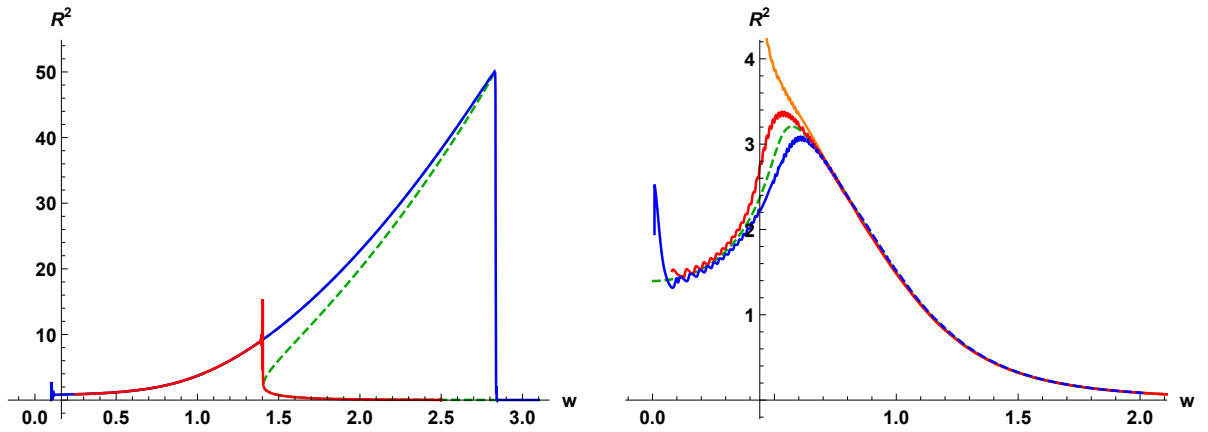

Figure A.4: Swept frequency response. Blue curve = up-sweep. Red curve = down-sweep. Green-dashed is theoretical curve $\sigma = 0$. Left: hardening resonator, $\epsilon = 0.05$ $\rho = 0.28$. Right: softening resonator $\epsilon = 0.8$, $\rho = -0.202$, $|\sigma| = \epsilon/400$. Orange curve = sweep down at $\rho = -0.225$

A.3 Flinch Instability

Fig. A.5, the counterpart to Fig. A.3 for the single-valued resonance, shows the maximum at much higher resolution. Oscillations of the amplitude appear around the maximum, but fade away to either side.

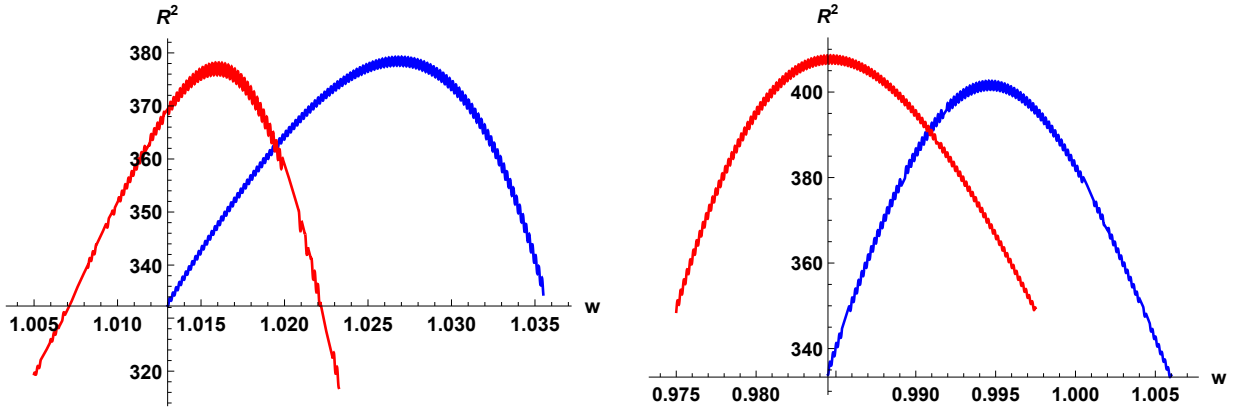

Figure A.5: Frequency sweep in vicinity of maximum with $\epsilon = 0.05$. Blue curve = up-sweep; red curve = down-sweep. Left: hardening resonator, $\rho = +0.00025$ Right: softening resonator, $\rho = -0.0001$.

Fig. A.6 is the counterpart to Fig. A.4-Left for the triple-valued resonance of a hardening resonator. In the up-sweep, oscillations begin prior to the jump down. However, there is no evidence of a flinch instability anticipating the jump-up in the down sweep. The large (damped) oscillations arise from the overshoot that occurs after the jump-up.

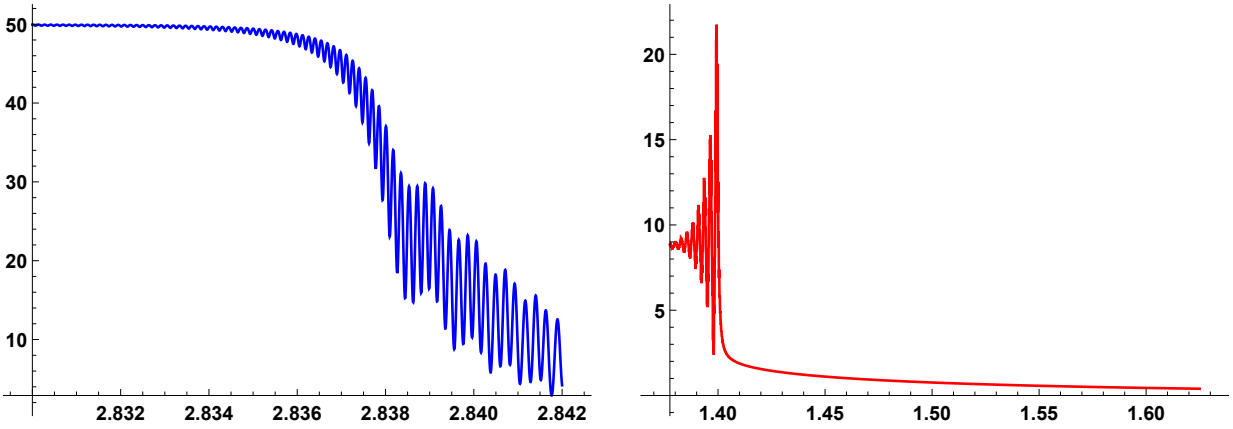

Figure A.6: Hardening resonator $\epsilon = 0.05$ $\rho = 0.28$. Left: up-sweep. Right: down-sweep.

Fig. A.7 is the counterpart to Fig. A.4-Right for the single-valued resonance of a softening resonator. For both the up-sweep and down-sweep, a flinch instability appears around the maximum and decays at either side.

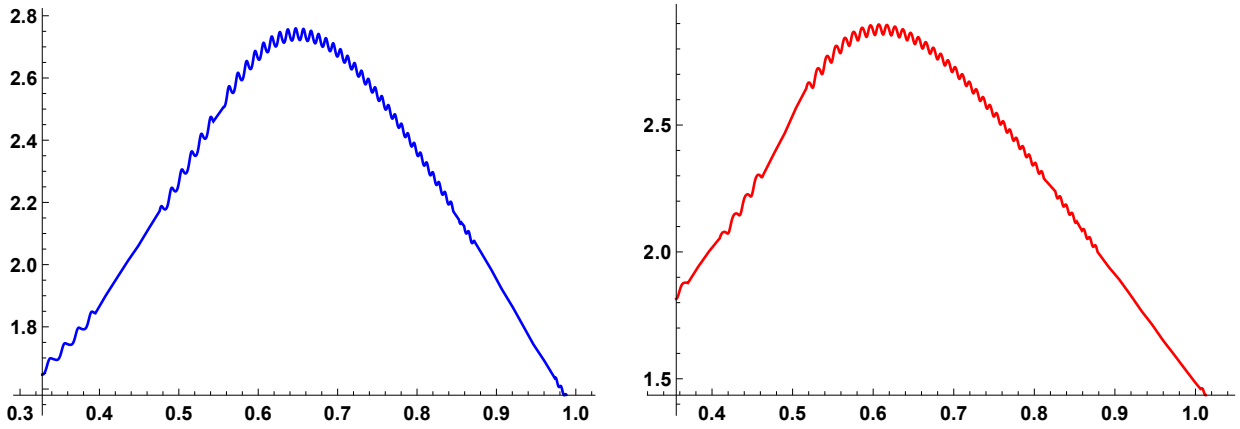

Figure A.7: Softening resonator $\epsilon = 0.8$ $\rho = -0.202$. Left: up-sweep. Right: down-sweep.

Appendix B

Commentary on Urabe's proof

An inhomogeneous differential equation (DE) contains a term that is not proportional to the unknown function or to any of its derivatives. This particular term is often called a forcing or a drive. For example, a loaded structural beam (and the equation that describes its displacement) is said to be forced (by the load). Another example is an oscillator driven by sinusoidal time-varying excitation. There are two (convergent) ways to think about finding solutions to a differential equation with sinusoidal forcing.

The first is to assume the solution is periodic and to expand the solution in a Fourier series $\sum_{n=0}^{N} a_n \cos nz + b_n \sin nz$. The Fourier series are a set of basis functions (or shape functions) that are orthogonal under the operation of multiplication followed by integration over the fundamental (i.e. longest) period. A Fourier series with unknown coefficients (a_n, b_n) is substituted into the DE. If the DE is linear, one may (A) simply inspect each of the terms $\cos nz, \sin nz$ to find the coefficients. Alternatively (B), the entire DE is multiplied by $\cos mz$ (or $\sin mz$) and integrated over the period; and the orthogonality properties will select a particular coefficient a_m (or b_m). If the DE is linear, we may rely on the existence, completeness, uniqueness and convergence properties[1] of Fourier series. If the DE is nonlinear in the unknown function, then there will be products of Fourier series; and finding the coefficients is no longer trivial. Fortunately, one can still appeal to method B: substitute the Fourier series into the EOM, multiply by each of the basis shapes and integrate over the period; this will convert the DE into a system of nonlinear algebraic equations for the coefficients. But the question arises: are the coefficients still unique and convergent? This is the question addressed by Urabe[18].

The second way to think about finding solutions to a forced DE is the *method of weighted residuals* (MWR). As before, a trial function composed of shape functions with unknown coefficients is substituted into the DE. The shape functions are not necessarily orthogonal or complete, which is why we do not call them basis functions. For example, they could be terms in a Maclaurin series $\sum_{n}^{N} a_n z^n$. In general, there will be a residual error; and we attempt to minimize it some way such that the coefficients become determined. In the MWR, the entire residual is multiplied by a weight function and then integrated over the domain of interest (in our case, the fundamental period). The choice of weight function gives a particular variety of MWR. In the Galerkin[2] MWR, the weight functions are the shape functions. Think of the shape functions as being degrees of freedom in different (abstract) directions. In such a case, multiplying by the weight and integrating will force the residual error to be orthogonal to the shape function. The residual error is minimized when there is no component of the residual error in the direction of each of the shape functions.

There is, of course, the case that the shape functions are true basis functions (and satisfy some DE and boundary conditions). When the shape functions are terms in a Fourier series, the two ways of thinking about finding a solution to a nonlinear DE with sinusoidal drive become one and the

[1] Which can be poor if the function to be represented is discontinuous in value or derivative.

[2] Boris Grigoryevich Galerkin (1871–1945) was a Soviet mathematician and an engineer.

same: use method B to setup a system of nonlinear algebraic equations (SNAE) for the coefficients. It is for this reason that Urabe[18, 19, 20] calls his Fourier series solution the Galerkin method.

The SNAE is the starting point for Urabe's proofs of existence and uniqueness. The proofs themselves depend upon properties of norms, the Jacobian of the SNAE, Green's function of linear operators, the Schwartz inequality, etc. The convergence proof is based on convergence of the SNAE solution under Newton iteration starting from the solution for the fundamental component when all other terms have been set (artificially) to zero. The present author has not verified (in detail) the Urabe proofs.

Urabe[18] investigates the steady state of a general nonlinear ODE with harmonic drive. Urabe demonstrates that as the order of the SNAE is increased (i.e. more Fourier harmonics are used), the solution converges to an exact periodic solution (i.e. the residual converges to zero). Urabe also demonstrates that the periodic solution is isolated, that is it has no neighbours and is unique. Both properties rely upon the Jacobian matrix of the SNAE being invertible. If the matrix determinant is zero, then it cannot be inverted and is described as *singular*. So the proofs are invalid in any region of the parameter space (of the Fourier coefficients) where the Jacobian determinant is zero. In the case of the MSR, and the fundamental Fourier component of the DR, there are parameter combinations where the determinant is zero; and the periodic solution ceases to be unique. These are the locations of $s = 0$ eigen-frequencies for the matrix $\mathbf{M}$ in Sec. 1.3 There is a related result. If we consider the eigen-frequencies of the system for small perturbations about the steady state. If the determinant of $\mathbf{M}$ is negative, then there is at least one eigen-solution $\exp(st)$ with $\Re[s] > 0$.

Appendix C

Dual-scales Explanation of Jump

Refs.[6, 11, 12] give similar mathematical explanation of the jump phenomena for the Duffing resonator. All of them use dual time scales, also known or fast and slow variables. The version due to Rand[12] is closest to the presentation herein, but the notation differs and we give additional results. The dual-scales are an example of a more general scheme: multiple-scales[4, 5]. The underlying idea is to consider the expansion representing the response to be a function of multiple independent variables (or scales). One begins by introducing new variables (of increasing slowness) by $v_n = \zeta^n t$ for $n = 0, 1, 2, \ldots$ and $0 < \zeta < 1$. In the variant below, we keep just two scales.

C.1 Derivation of slow flows

The starting point is Eq. 1.3 with $\beta\langle x^2\rangle x$ replaced by βx^3. It is customary to introduce a parameter $0 \leq \zeta \leq 1$ that is both a smallness and an order parameter.

$$\alpha x + \ddot{x} \;=\; \zeta[\gamma\cos\omega t \;-\delta\dot{x} \;-\beta x^3]\;. \tag{C.1}$$

If $\zeta = 0$ we have a free, undamped harmonic oscillator (SHO). If $\zeta = 1$, we recover the original equation. Later we shall seek a solution of Eq. C.1 in the form of a power series in ζ (called a Poincaré expansion). In such a case, ζ facilitates keeping track of the order of the expansion.

The key step is to introduce the two time scales; this will convert Eq. C.1 into a partial differential equation (PDE). In particular, this will increase the types of function that satisfy the left-hand side of Eqs. C.1 and C.4. Let $z = \omega t$ be the fast variable, and $v = \zeta t$ be the slow variable. Here $\omega > 0, \zeta > 0$ and $\omega \gg \zeta$. Notice, in contra-distinction to Sec. 1.1.4, z is normalized time in units of inverse drive frequency ω. With these dual variables, time derivatives have to be re-expressed as mixed derivatives; as follows:

$$x(t) \to x(z,v), \qquad \frac{dx}{dt} \to \omega\frac{dx}{dz} + \zeta\frac{dx}{dv}, \qquad \frac{d^2x}{dt^2} \to \omega^2\frac{d^2x}{dz^2} + 2\omega\zeta\frac{d}{dz}\frac{d}{dv}x + \zeta^2\frac{d^2x}{dv^2}\;. \tag{C.2}$$

The mixed derivatives replace the operators in Eq. C.1, resulting in a PDE for $x(z,v)$. The next step is to introduce the power series: $x(z,v) \to X(z,v) + y(z,v)\zeta$. X is zeroth order; y is first order. The strategy is to set X equal to the product of a slowly varying function and a sinusoidal carrier waveform, and find conditions such that X remains the dominant term despite the circumstance that X will provide a forcing of y. The combination $X + \zeta\, y$ is inserted in the EOM and acted upon by the mixed derivatives.

Next there is a slight of hand: we set $\alpha = \omega^2 - \zeta\,\Delta$. Provided that the detuning (or split) $\Delta \neq 0$, this says that the resonance frequency is close to (but distinct from) the drive frequency. Introducing ζ into the detuning will perform the magic trick of removing Δ from the left-hand side of Eqs. C.4, C.5. The next step is to truncate the EOM to first order in ζ, leading to

$$\omega^2\left[X + \frac{d^2X}{dz^2}\right] + \zeta\left[2\omega\frac{d}{dz}\frac{d}{dv}X - \Delta X\right] + \zeta\omega^2\left[y + \frac{d^2y}{dz^2}\right] \;=\; \zeta\left[\gamma\cos z - \omega\delta\frac{dX}{dz} - \beta X^3\right]\;. \tag{C.3}$$

Evidently, this is really two simultaneous equations separated by the order parameter:

$$\omega^2 \left[X + \frac{d^2X}{dz^2} \right] = 0 \tag{C.4}$$

$$\omega^2 \left[y + \frac{d^2y}{dz^2} \right] = \left[\Delta X - 2\omega \frac{d}{dz}\frac{d}{dv} X \right] + \left[\gamma \cos z - \omega\delta \frac{dX}{dz} - \beta X^3 \right] . \tag{C.5}$$

Eq. C.4 has the general solution $X(z, v) = A(v) \cos z + B(v) \sin z$. Note here that the "constants" of integration A, B are in fact arbitrary functions of slow time because Eq. C.3 is a PDE. [Had we not introduced the dual-time variables, we would have a different system of equations with the only solution A and B equal to constants.] Note also that the phase z accumulates quickly, whereas the argument v of the amplitude functions (A, B) increments slowly with respect to the clock-time t.

The solution $X(z, v)$ is inserted into the right-hand side of Eq. C.5; and it may drive $y(z, v)$ because they are resonant. Ideally, the slower function X remains the dominant term, over powering the faster oscillating function y. The cubic term X^3 also contains resonant drive terms, as may be found by expansion:

$$\begin{aligned} (A\cos z + B \sin z)^3 &= (3/4)\left[(A^3 + AB^2)\cos z + (B^3 + A^2B)\sin z\right] \\ &\quad +(1/4)\left[(A^3 - 3AB^2)\cos 3z - (B^3 - 3A^2B)\sin 3z\right] . \end{aligned}$$

The expansion is inserted in the right-hand of Eq. C.5. We then compare coefficients of $\cos z$ and $\sin z$, and set all the resonant drive terms equal to zero. This yields two simultaneous equations for the evolution of A and B:

$$2\omega B'(v) + \omega\delta\, B - \Delta \times A + (3/4)\beta A(A^2 + B^2) = \gamma \tag{C.6}$$

$$2\omega A'(v) + \omega\delta\, A + \Delta \times B - (3/4)\beta B(A^2 + B^2) = 0 . \tag{C.7}$$

These are the *slow flows*. Here X' denotes the derivative $dX(v)/dv$.

C.1.1 Solution of residual for y

The non-resonant terms result in a residual forcing:

$$\omega^2 \left[y + \frac{d^2y}{dz^2} \right] = -(1/4)\beta A(A^2 - 3B^2)\cos 3z + (1/4)(B^2 - 3A^2)\sin 3z . \tag{C.8}$$

Here $A(v)$ and $B(v)$ are independent of z. The general solution of Eq. C.8 is:

$$\begin{aligned} y(z, v) &= (C_1 \cos z + S_1 \sin z) \\ &+ \left[A(A^2 - 3B^2)(2\cos z + \cos 3z) + B(3A^2 - B^2)(2\sin z + \sin 3z)\right] \beta/(32\omega^2) . \end{aligned}$$

where the constant C_1, S_1 are chosen to satisfy initial conditions.

C.1.2 Fixed & turning points of X

An exhaustive account of the nature of fixed points of ODE's in one, two and three spatial dimensions is given by Arnold[30]. But we need only simple properties for one dimension. The fixed points (FP) of the motion $A(v)$ and $B(v)$, and the nature of these FPs, characterise the motion. The FPs may be either elliptic (centres) or hyperbolic (saddles). The fixed points are the solutions for (A, B) of Eqs. C.6 and C.7 with the derivatives set to zero $(A', B') = (0, 0)$. The fixed-point relations are

$$\gamma + A\Delta = (3/4)\beta A R^2 + B\omega\delta \quad \text{and} \quad B\Delta = (3/4)\beta B R^2 - A\omega\delta . \tag{C.9}$$

In general, the roots consist of three pairs (A, B): one real pair and two complex pairs, or three real pairs. The quantity $A^2 + B^2 \equiv R^2$ is ubiquitous; and if it's values are known (there are 1 or 3 of them), then the general case roots are

$$\pm A = \frac{4\gamma\kappa}{\kappa^2 + (4\omega\delta)^2}, \qquad B = \frac{16\gamma\,\omega\delta}{\kappa^2 + (4\omega\delta)^2}, \quad \text{with} \quad \kappa \equiv (3\beta R^2 - 4\Delta)\ . \tag{C.10}$$

Until this point, the frequency split parameter Δ has an arbitrary value. However, from the fixed-point relations Eq. C.9, it should be evident that Δ and R^2 are related. Eqs. C.9 are manipulated[1] to produce $(3R^4\beta - 4R^2\Delta)^2 + 16[(R^2\omega\,\delta)^2 - (R\,\gamma)^2] = 0$ which may be solved for $R^2(\Delta)$. Alternatively, as before, we may invert the cause Δ and effect R (because time ordering is lost in the steady state) and solve for

$$\Delta \ = \ (3/4)\beta R^2 \ \pm \sqrt{(\gamma/R)^2 - \delta^2}\ . \tag{C.11}$$

Δ sets the drive frequency $\omega^2 = \alpha + \zeta\,\Delta$; because, in a particular system, the zero-amplitude resonance frequency α is a constant. The two values of Δ for a given value of R correspond to the middle and upper branches. When $\beta > 0$, the positive sign gives the middle branch. When $\beta < 0$, the negative sign gives the middle branch. The condition that Δ be real, leads to the bounding inequality $R^2 \le (\gamma/\delta)^2$. At this value there is a single value of Δ that locates the resonance maximum.

A condition for turning points is given by setting $d\Delta/R = 0$.

$$\frac{d\Delta}{dR} \ = \ \frac{3}{2}R\beta \ \pm \frac{\gamma}{R^2\sqrt{1 - (R\delta/\gamma)^2}}\ . \tag{C.12}$$

Here the value of R has to be consistent with Eq. C.9. There are two TPs (solutions of $d\Delta/dR = 0$) because $R = \pm\sqrt{A^2 + B^2}$ may be positive or negative. For the hardening resonator ($\beta > 0$), R is positive (negative) on the upper (lower) branch. For the softening resonator ($\beta < 0$), R is negative (positive) on upper (lower) branch.

C.2 Lossless resonator

We can imagine plotting the location of the (real) roots in the plane (A, B). In the limit of very weak damping, the fixed points move to the line $B = 0$. The appropriate conditions are $\omega\delta \ll 1$ much less than all the quantities $|\Delta|$ and $|\gamma|$ and $|\beta|R^2$. The fixed point condition becomes $\gamma + A\Delta = (3/4)\beta A^3$ (because $A = \pm R$). In this limit, there are three fixed points; at each of them $B = 0$, and the values of A are

$$A_1 = \frac{2^{1/3}Z}{3\beta} + \frac{2\times 2^{2/3}\Delta}{3Z},\ A_2 = -\frac{(1 - i\sqrt{3})Z}{3\times 2^{2/3}\beta} - \frac{2^{2/3}(1 + i\sqrt{3})\Delta}{3Z},\ A_3 = -\frac{(1 + i\sqrt{3})Z}{3\times 2^{2/3}\beta} - \frac{2^{2/3}(1 - i\sqrt{3})\Delta}{3Z}\ .$$

with $Z = [9\beta^2\gamma + \sqrt{81\beta^4\gamma^2 - 16\beta^3\Delta^3}]^{1/3}$. The radicand within Z is the cubic determinant. The condition for three roots is $\beta^3(81\beta\gamma^2 - 16\Delta^3) < 0$. Thus the threshold value of detuning is $\Delta = \text{sign}[\beta](3/2)(3/2)^{1/3}(\beta\gamma^2)^{1/3}$.

When $\delta = 0$, relation Eq. C.11 becomes $\Delta = (3/4)\beta A^2 \ \pm \gamma/A$; for a particular value of A^2 the two values of Δ are middle and upper branches. When $\delta = 0$, Eq. C.12 becomes $d\Delta/dA = (3/2)A\beta \ \pm \gamma/A^2$. It might appear that the condition $d\Delta/dA = 0$ generates two turning points. But this is not the case, because A has to be chosen consistent with $\gamma + A\Delta = (3/4)A^2\beta$. Only one value of A is consistent with both equations, and it is the lower turning point.

[1] The first $\times B$, the second $\times A$, are subtracted to give one Eqn. The first $\times A$, the second $\times B$, are added to give another Eqn. And then squares of parts of the Eqns. are equated.

C.2.1 Movement of fixed points

Starting from $A_{1,2,3}$ we may find an approximation to the FPs when $\delta \neq 0$ using the method of Newton iteration. The two Eqs. C.9 are each of the form $F_i(A, B, \delta) = 0$ with $i = 1, 2$. At the approximate fixed points $(A_0, B_0, 0)$, when $\delta \neq 0$, there are residuals R_i. Thus $F_i(A_0, B_0, 0) - R_i = 0$. Suppose there is an exact solution $F_i(A_0 + a, B_0 + b, \delta) = 0$. We make a Taylor expansion to first order in the increments (a, b). Thus $F_i(A_0, B_0, 0) + a(\partial F_i/\partial A) + b(\partial F_i/\partial B) \approx 0$ where the derivatives are evaluated at (A_0, B_0). Prior to taking the derivatives, R^2 is replaced by $(A^2 + B^2)$. The two equations for F_i may be combined to eliminate $F_i(A_0, B_0, 0)$, leading to simultaneous equations for $[a, b]$. In the particular, evaluated at $(A, B = 0)$, the solution for the increment simplifies to $[a, b] = [0, 4A\omega\delta/(3A^2\beta - 4\Delta)]$. The details are given in Sec. C.4.

Note, Newton iteration may be called Newton-Raphson-Simpson iteration in honour of the original creator (Isaac Netwon, 1685) and major contributors Joseph Raphson (1690) and Thomas Simpson (1740). The calculus-based version used in the modern day is due to Simpson (1710-1761); he is also the originator of Simpson's rules for numerical integration of definite integrals.

C.2.2 Nature of fixed points

Consider the slow-flow Eqs. C.6, C.7 in the limit the oscillator is lossless $\delta \to 0$. Precisely at the FPs, the flows are of the form $[A(v), B(v)] = [A_i, 0]$ with $i = 1, 2, 3$ and $[A', B'] = [0, 0]$. We make a small-amplitude expansion about the fixed point: $A(v) = A_i + a(v)$ and $B(v) = 0 + b(v)$. These functions are substituted in Eqs. C.6, C.7, and the expressions linearized yielding an ODE for $a(v), b(v)$. The details are given in Sec. C.4. We substitute a trial solution of the form $\exp(sv)$, leading to an eigenvalue equation for s: $(8\,s\,\omega)^2 + (-9A^2\beta + 4\Delta) \times (-3A^2\beta + 4\Delta) = 0$. The situation $s = 0$ has the trivial solution $(a, b) = (0, 0)$.
When $s^2 > 0$ there are hyperbolic solutions:

$$\begin{aligned} a(v) &= c_1 \cosh(sv) + c_2 \sinh(sv) \times (+3A^2\beta - 4\Delta)/(8s\omega) \\ b(v) &= c_2 \cosh(sv) + c_1 \sinh(sv) \times (-9A^2\beta + 4\Delta)/(8s\omega)\ . \end{aligned}$$

When $s^2 < 0$ there are elliptic solutions:

$$\begin{aligned} a(v) &= c_1 \cos(sv) + c_2 \sin(sv) \times (+3A^2\beta - 4\Delta)/(8s\omega) \\ b(v) &= c_2 \cos(sv) + c_1 \sin(sv) \times (-9A^2\beta + 4\Delta)/(8s\omega) \quad \text{and} \quad s \equiv |s|\ . \end{aligned}$$

When $\Delta = 0$, the FPs are centres of oscillation with local frequency $|s| = 3\sqrt{3}A^2\beta/(8\omega)$.
Consider again the condition for elliptic (stable) FPs, $s^2 < 0$, or $(-9A^2\beta + 4\Delta) \times (-3A^2\beta + 4\Delta) > 0$. We may eliminate Δ using expression Eq. C.11. At the fixed points, $A = \pm R$ and $\delta = 0$. Hence the condition for a stable centre of oscillation is:

$$2\frac{\gamma^2}{A^2} \pm 3A\beta\gamma > 0\ . \tag{C.13}$$

For the hardening resonator, with $\beta > 0$, two possible conditions for a centre are:

$$A > 0 \quad \text{or} \quad A < 0\ \&\ 0 < \beta < -2\gamma/(3A^3)\ .$$

For the softening resonator, with $\beta < 0$, two possible conditions for a centre are:

$$A < 0 \quad \text{or} \quad A > 0\ \&\ -2\gamma/(3A^3) < \beta < 0\ .$$

If the conditions are violated, then the fixed point is a saddle.

C.3 Slow motion and Hamiltonian

The concluding part of the jump explanation, is to explore the slow motion (governed by Eqs. C.6 and C.7) as the parameters β and Δ are varied. Without loss of generality, we set $\alpha = 1$ and the excitation frequency $\omega \approx 1$. Initially, we shall set the damping constant $\delta = 0$. This facilitates deriving the flows A' and B' from a Hamiltonian $H(A, B)$, and visualizing the flows in the phasenraum (phase space) of A, B. When the system is conservative, the Hamiltonian formulation enables us to visualize the motion without solving for the time dependence of either $A(v)$ or $B(v)$. We plot B against A, and neither know nor care what is the time v.

For brevity let $R^2 = (A^2 + B^2)$. The equations of motion:

$$dA/dv = [+3\beta BR^2 - 4B\Delta]/8 \equiv \partial H/\partial B \quad dB/dv = [-3\beta AR^2 + 4A\Delta + 4\gamma] \equiv -\partial H/\partial A \,,$$

$$\text{are derived from the Hamiltonian} \qquad H(A, B) = (3\beta R^4 \; - 8R^2\Delta \; - 16A\gamma)/32 \,. \qquad \text{(C.14)}$$

The flow lines (i.e. curves), also called stream lines, are contours of constant Hamiltonian value. The fixed points of the Hamiltonian flows are the solutions for (A, B) of $(A', B') = (0, 0)$, and are discussed above. Flow lines encircle elliptic points. Almost all flow lines near a hyperbolic point are repelled away; four lines only either emerge from or converge on it. Depending on the values of A_i there may be one or three fixed points; and they may be of different type depending on the values of γ, β, Δ. The large scale flow pattern has to reconcile the presence of elliptic and hyperbolic FPs. When there are two elliptic points and one saddle point, one of the stable regions is (vastly) distorted from a circle and is wrapped around the other circular stable region. The wrapped region resembles a letter C; and where the opposite arms of the C-region touch (to form an O) there is a saddle point. The very fine-structured nature of bifurcations can make it difficult to state precisely from where a jump commenced. Nayfeh[5] suggests to use the Lyapunov function to clarify precisely the extent of the basins of attraction.

There are a couple of peculiarities that we need to be aware of. Foremost, the absence of dissipation implies that the resonance curve has no maximum; and this implies the location of the jump-down is somewhat arbitrary. It must occur where the resonance curve is canted over and triple valued. For the hardening (softening) resonator it must occur at a frequency above (below) the jump-up; and it occurs at a frequency where the amplitude on the middle and upper branches is approximately equal; but that is all we can say, we cannot be more precise.

The second oddity is that locally about a fixed point in the (A, B) plane, the sign (polarity) of the Hamiltonian changes across the resonance. Suppose the Hamiltonian is considered a surface. If the topography of the dominant FP is a bowl well below resonance, then the landscape of the dominant FP is a dome well above resonance. Fortunately, the nature of the fixed points is invariant with respect to mirroring of the Hamiltonian. This property is explained in Sec. C.5.

When the motion is lossless, the flow lines are all we need to know. When there is dissipation, the motion will have a small component perpendicular to the contours and that points toward the dominant elliptic fixed point (whether it is a bowl or dome does not matter). Later, we shall overlay selected trajectories to illustrate the effect of small damping on the long time scale.

C.3.1 Hardening resonator

The value of Δ sets the drive frequency either below ($\Delta < 0$) or above ($\Delta > 0$) the nominal resonance frequency α. Imagine increasing Δ at constant value of the nonlinear parameter β. We shall encounter three FPs, arranged from negative to positive as $[A_k, \; A_j \; A_i]$. Well below resonance, there is a single real valued fixed point; and it is a centre at $0 < A_i \approx 0$. As Δ is increased, so A_i grows in size. Slightly above resonance, the ellipse-shaped flow lines begin to distort; and a second feature begins to emerge at $A < 0$. At the critical value the $A_j = A_k$ and the FP is both a centre and saddle. As $\Delta > 0$ is increased beyond a critical value, three real fixed points emerge: a centre at $A_i > 0$, another centre at $A_j < 0$ and a saddle at $A_k < A_j$. The local sense of rotation

is clockwise around A_i, and counter-clockwise at A_j. A_i is the upper branch, A_j the lower branch, and A_k the middle branch. The distinct FPs satisfy $|A_i| > |A_j|$; and the flow lines will carry the state of the oscillator $[A(v), B(v)]$ from the lower to the upper branch. Suppose we continue to increase Δ. Three FPs become more distinct. The centre $A_j \to 0$. The saddle $|A_k| < A_i$. The stable region centred on A_j grows. The stable region centred on A_i distorts into a reversed C; the arms of the C meet at the saddle. Suppose we continue to increase Δ. It remains that $A_i > 0$ and $A_k < 0$; but $|A_k| \leftrightarrow A_i$ and the modulus of both increases; and they become equal at the maximum of the resonance. The lower branch $A_j \to 0$. The distorted stable region with origin at A_i encloses the circular stable region centred on A_j. Dissipation will carry the oscillator state down hill from the outer to the inner stable region (i.e. from the upper to the lower branch).

Toward DC, the centre is the single real positive root $A_i > 0$. Because $\delta = 0$, there are three real roots in the asymptotic regime ($\omega^2 \gg \alpha$). The true stable centre (lower branch) is $A_j < 0$ and $|A_j| \to 0$. There is a bogus second centre in the asymptotic regime at $A_i > 0$; it is one of the pair of values on the upper (A_i) and middle (A_k) branches which are almost of equal modulus but opposite in sign.

C.3.2 Softening resonator

We shall imagine first that the excitation frequency is well above the resonance frequency, and that Δ is progressively reduced; starting at a positive value, and ending at a negative value (i.e below the nominal resonance of the softening resonator). We shall encounter three FPs, arranged from negative to positive as $[A_i, A_j, A_k]$. When all branches are present, A_i is the upper, and A_j the lower, and A_k the middle branch.

At $\Delta > 0$, there is a single real root $0 > A_i \approx 0$ and it is a centre of oscillation, leading to flow lines of circulation (around the root) in the (A, B) plane. The modulus $|A_i|$ diminishes toward zero as $\Delta > 0$ increases. However, we shall consider smaller values of Δ such that A_i becomes more negative. When $\Delta = 0$, there is a single real root with flows circulating about it; but the flowlines start to become asymmetric. As Δ becomes negative, the asymmetry becomes more pronounced. A_i remains negative but its modulus further increases. If Δ becomes more negative, the flowlines distort in a way that signals the emergence of an additional fixed point at $A > 0$. At the threshold value of Δ there are three real roots: one of them $A_i < 0$ is distinct, and the other two $A_j = A_k > 0$ are coincident. At threshold, this coincident double root has both elliptic and hyperbolic character. As Δ is made more negative, the coincident roots separate into a hyperbolic fixed point A_k and a second centre A_j. The roots satisfy $0 < A_j < A_k < |A_i|$. If Δ is reduced more there is jump up from the lower branch or middle branch. As Δ is further reduced, the oscillation centre $A_j > 0$ moves toward zero; and the other two roots (one a centre, and one a saddle) become almost equal in modulus, but remain of opposite sign. Thus $A_i < 0 < A_j < A_k$ and $A_k \to |A_i|$. The flowlines circulating around A_i distort into a C-shape that encloses the centre of rotation at A_j. The arms of the C-shape form outward flowing branches from the saddle point. When dissipation is present, trajectories that begin in the C-shaped region spiral inward to the centre at $A_j \approx 0$. This is the collapse of amplitude (or jump-down) that occurs as the drive frequency is swept from high to low frequency. In doing so, they may reverse their direction of rotation.

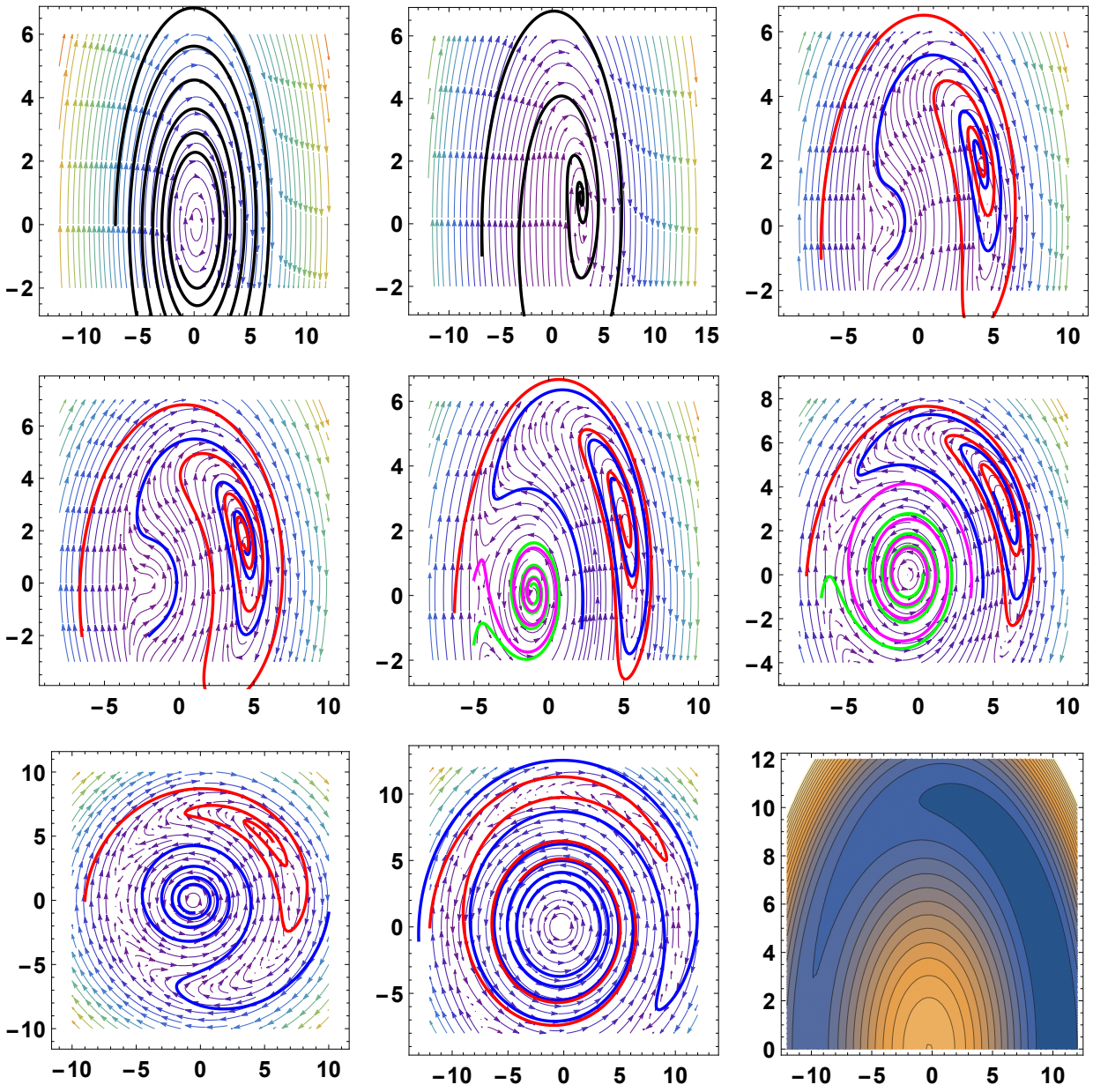

Figure C.1: (A, B) Phase space for hardening resonator. Rainbow curves with arrow heads are flow lines when $\delta = 0$. Other curves for $\delta = 0.01$. $F_{1,1}$: $\Delta = -0.5$ single real root and stable centre of oscillation. $F_{1,2}$: $\Delta = 0$ single real root and stable centre of oscillation. $F_{1,3}$: $\Delta = 0.06$ single real fixed point is upper branch; nascent lower and middle branches. $F_{2,1}$: $\Delta = 0.06326$ threshold for three real roots, two of which are equal; jump-up from junction of lower and middle branches. $F_{2,2}$: $\Delta = 0.10$ three distinct real roots (i.e branches); jump up from middle or lower branch. $F_{2,3}$: $\Delta = 0.15$ three distinct real branches; jump up from middle or lower branch. $F_{3,1}$: $\Delta = 0.20$ three distinct fixed points; jump down from upper to lower branch; possible jump up from middle branch. $F_{3,2}$: $\Delta = 0.40$ three distinct fixed points; jump down from upper to lower branch. $F_{3,3}$: $\Delta = 0.40$ height map of Hamiltonian shows hill surrounded by moat.

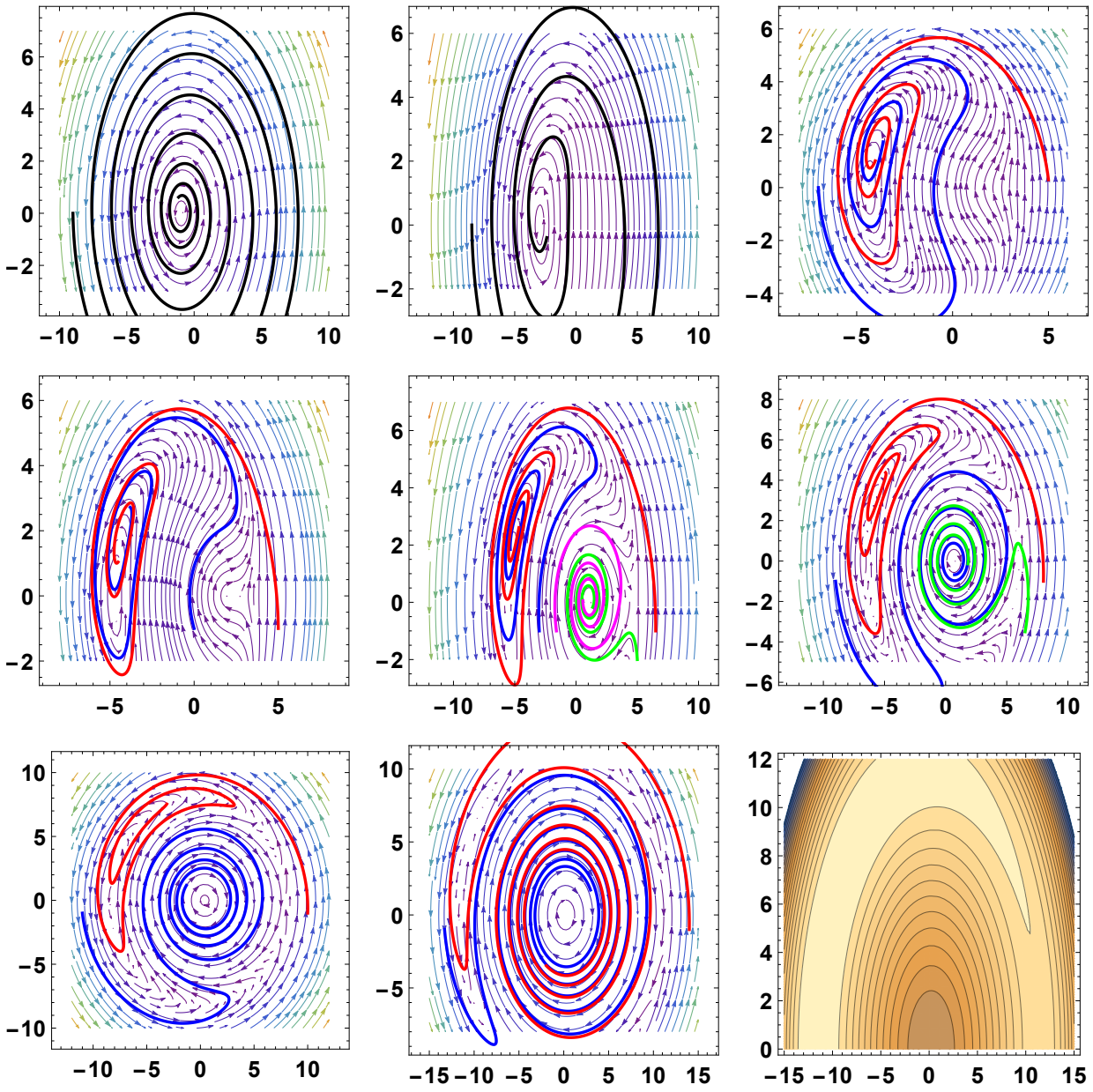

Figure C.2: (A, B) Phase space for softening resonator. Rainbow curves with arrow heads are flow lines when $\delta = 0$. Other curves for $\delta = 0.01$. $F_{1,1}$: $\Delta = 0.5$ single real root and stable centre of oscillation. $F_{1,2}$: $\Delta = 0$ single real root and stable centre of oscillation. $F_{1,3}$: $\Delta = -0.05$ single real fixed point is upper branch; nascent lower and middle branches. $F_{2,1}$: $\Delta = -0.06326$ threshold for three real roots, two of which are equal; jump-up from junction of lower and middle branches. $F_{2,2}$: $\Delta = -0.10$ three distinct real roots (i.e branches); possible jump up from middle branch. $F_{2,3}$: $\Delta = -0.15$ three distinct real branches; jump up or jump down from middle branch. $F_{3,1}$: $\Delta = -0.25$ three distinct fixed points; jump down from middle to lower branch. $F_{3,2}$: $\Delta = -0.50$ three distinct fixed points; jump down from upper to lower branch. $F_{3,3}$: $\Delta = -0.50$ height map of Hamiltonian shows bowl with rim that folds over to negative values.

C.4 Jacobian matrix & determinant

The Jacobian is the determinant of the matrix of the first order partial derivatives of the mapping between two N-dimensional spaces. It is named after Carl Gustav Jacobi (1804–1851) whose memoir[31] on functional determinants was published in 1841. Brezis[32] outlines the history. The Jacobian arises in the transformation of surface and volume elements (dS, dV) between coordinate systems, and when Newton iteration is used to solve a system of simultaneous algebraic equations. We illustrate the use of the Jacobian matrix and its determinant by two closely related examples.

The two slow flow Eqs. C.6 and C.7 are of the form $F_i(A, B, A', B', \delta) = 0$ where $i = 1, 2$. Let us find a linear mapping to the neighbouring location $G_i(A+a, B+b, A'+a', B'+b', \delta+d) = 0$. We make a Taylor expansion about the origin point, and linearize in the small quantities a, b, a', b', d.

$$G_i \approx F_i \; + \; a\,\partial F_i/\partial A + b\,\partial F_i/\partial B + a'\partial F_i/\partial A' + b'\partial F_i/\partial B' + d\,\partial F_i/\partial\delta \approx 0 \; .$$

But $F_i = 0$. The result may be written in matrix form: $\mathbf{J}\mathbf{x} + \mathbf{K}\mathbf{x}' + d\,\mathbf{R} = \mathbf{0}$ where

$$\mathbf{J} = \begin{bmatrix} \partial F_1/\partial A & \partial F_1/\partial B \\ \partial F_2/\partial A & \partial F_2/\partial B \end{bmatrix}, \quad \mathbf{x} = \begin{bmatrix} a \\ b \end{bmatrix}, \quad \mathbf{K} = \begin{bmatrix} \partial F_1/\partial A' & \partial F_1/\partial B' \\ \partial F_2/\partial A' & \partial F_2/\partial B' \end{bmatrix}, \quad \mathbf{x}' = \begin{bmatrix} a' \\ b' \end{bmatrix}, \quad \mathbf{R} = \begin{bmatrix} \partial F_1/\partial\delta \\ \partial F_2/\partial\delta \end{bmatrix} .$$

Each of $\mathbf{J}$ and $\mathbf{K}$ are Jacobian matrices. We could have written the equation in terms of a single matrix and an extended vector $\mathbf{x} = [a, b, a', b']$, but the matrix would in this particular case be in block form. We now consider two variants.

C.4.1 Nature of fixed points

Suppose F_i are the equations for a fixed point, that is $F_i(A, B, 0, 0, \delta) = 0$; and that we wish to characterise the motion nearby, that is $G_i(A + a, B + b, a', b', \delta)$. We replace the vector $\mathbf{x}'$ by its Laplace transform $s\mathbf{x}$. The matrix equation becomes $\mathbf{M}\mathbf{x} = (\mathbf{J} + s\mathbf{K})\mathbf{x} = \mathbf{0}$. This is an eigenvalue equation for s. It has non-trivial solutions if the determinant of $\mathbf{M}$ is zero. We use the slow flow equations to evaluate the partial derivatives. Hence the matrices:

$$\mathbf{J} = \begin{bmatrix} (-3/4)(3A^2 + B^2)\beta + \Delta & -(3/2)AB\beta - \omega\delta \\ -(3/2)AB\beta + \omega\delta & -(3/4)(A^2 + 3B^2)\beta + \Delta \end{bmatrix} \quad \text{and} \quad \mathbf{K} = \begin{bmatrix} 0 & -2\omega \\ +2\omega & 0 \end{bmatrix} .$$

The determinant is

$$D = (27/16)R^4\beta^2 - 3R^2\beta\Delta + \Delta^2 + (2s + \delta)^2\omega^2 \quad \text{with} \quad R^2 \equiv (A^2 + B^2) \; .$$

The two solutions of $D = 0$ are: $s = -\delta/2 \pm \sqrt{-(3R^2\beta - 4\Delta)(9R^2\beta - 4\Delta)}$. The motion becomes unstable when $s = 0$, which occurs when the detuning falls between the thresholds

$$\Delta = [6R^2\beta \pm \sqrt{9R^4\beta^2 - (4\omega\delta)^2}]/4 \tag{C.15}$$

In the special case $\delta = 0$, the fixed points move to the line $B = 0$. The eigen frequencies become $s\,\omega = \pm\sqrt{-(3A^2\beta - 4\Delta)(9A^2\beta - 4\Delta)}$ and the motion is unstable in the detuning range $\Delta = (3/4)A^2\beta$ to $\Delta = (9/4)A^2\beta$. Here, of course, A is not a free parameter; it must be chosen consistent with the cubic equation for FPs and is found to lie on the middle branch.

C.4.2 Movement of fixed points

Starting from the lossless condition $\delta = 0$, we may use the Jacobian matrix to estimate where the fixed points move to when the resonator becomes lossy and δ assumes a small non-zero value. At the FPs, $\mathbf{x}' = \mathbf{0}$. Hence the matrix equation becomes $\mathbf{J}\,\mathbf{x} + d\,\mathbf{R} = \mathbf{0}$. The equation is solved by pre-multiplying by the matrix inverse $\mathbf{J}^{-1}$. Thus $\mathbf{x} = -d\,\mathbf{J}^{-1}\mathbf{R}$ provided the Jacobian determinant is non-zero. The partial derivatives are performed first, and then Jacobian matrix and residual $\mathbf{R}$

are evaluated at $(A, B, A', B', \delta) = (A, 0, 0, 0, 0)$. $\mathbf{R} = [-B\omega, +A\omega]$ becomes $[0, A\omega]$. Also $d \to \delta$. Hence the increment

$$\begin{bmatrix} a \\ b \end{bmatrix} = \delta \begin{bmatrix} \frac{4}{-9A^2\beta+4\Delta} & 0 \\ 0 & \frac{4}{-3A^2\beta+4\Delta} \end{bmatrix} \cdot \begin{bmatrix} 0 \\ -A\omega \end{bmatrix} = \begin{bmatrix} 0 \\ \frac{4A\omega\delta}{3A^2\beta-4\Delta} \end{bmatrix} . \tag{C.16}$$

C.5 Mirror Hamiltonian

The second oddity concerns a property of the Hamiltonian, best illustrated by two examples. Consider the harmonic oscillator Hamiltonian $H = p^2/2 + x^2/2$. There is an elliptic FP at $x = 0$ which is the centre of a bowl and clockwise rotating flow. If we introduce dissipation such that $\dot{p} + x + \dot{x}\delta = 0$, the motion will descend the bowl and will spiral inward (in the x, p plane) to the FP. Suppose we make the mirror transformation $H \to -H$, such that the bowl becomes a dome. There is a counter-clockwise rotation around the top of the dome. Under dissipation, does the motion still fall downwards, and thus spiral outwards in the x, p phase plane? The answer is emphatically *no*. The analogy to topography, bowl versus dome, is misleading and irrelevant. The nature of the fixed point(s) is invariant with respect to change of sign of the Hamiltonian: the flowline continues to spiral inward to the elliptic fixed point. The explanation is thus. Viewed from above, the original Hamiltonian resembles a bowl; whereas viewed from beneath (looking upward from underneath) the same 3-D shape appears as a dome. From these two different view points, the sense of rotation appears opposite (even though the motion itself has not changed). We may liken this to an analog clock with a transparent dial. Viewed face on, the hands move clockwise; viewed from behind, the hands appear to move anti-clockwise.

Consider the pendulum Hamiltonian $H = p^2/2 + (1 - \cos x)$. The equations of motion are $\dot{x} = \partial H/\partial p = p$ and $\dot{p} = -\partial H/\partial x = -\sin x$. There is an elliptic FP at $x = 0$ which is the centre of a bowl and clockwise rotating flow, and hyperbolic FP at $x = \pm\pi$ which are the locations of saddle points such that $p = 0$ is the direction of descent and $x = \pm\pi$ are directions of ascent. If we make the mirror transformation $H \to -H$, the flow lines are identical with those of the original. However, the directions of flow are reversed; for example counter-clockwise rotation about the FP at $x = 0$. And the topography is reversed: the bowl becomes a dome; and the directions uphill and downhill from the saddle point are interchanged. Nevertheless, the flow lines are identical and, moreover, the nature of the fixed points is unchanged. Thus when dissipation is introduced, $\dot{p} + \sin x + \dot{x}\delta = 0$, motion is attracted to the elliptic FP and repelled by the hyperbolic FP irrespective of whether it is bowl or dome, or valley or mountain ridge.

In the case of the driven anharmonic oscillator, we find as follows. For the hardening resonator below resonance the FP at $A > 0$ and $|A| \approx 0$ is centre of a bowl, and the asymptotic response well above resonance has a FP at $A < 0$ and $|A| \approx 0$ that is a dome. Nevertheless, they are both centres of rotation (clockwise and counter-clockwise, respectively). And, moreover, when dissipation is introduced the flowlines will be pulled toward these FPs in both cases. The *key point is* <u>*not*</u> to think of the system state (A, B) as falling down hill when energy dissipation is added to complete the description. For the softening resonator above resonance the FP at $A < 0$ and $|A| \approx 0$ is centre of a dome, and the response well below (the nominal small-amplitude) resonance frequency has a FP at $A > 0$ and $|A| \approx 0$ that is centre of a local basin. The sense of rotation is reversed between these cases (counter-clockwise and clockwise, respectively).

Bibliography

[1] M. M. Karliner, V. E. Shapiro, and I. A. Shekhtman: Instability in the Walls of a Cavity Due to Ponderomotive Forces of the Electromagnetic Field, Sov. Phys. Technical Physics **11** (1967) pp. 1501-1507.

[2] Georg Duffing: Erzwungene Schwingungen bei veränderlicher Eigenfrequenz und ihre technische Bedeutung, Heft 41/42. Vieweg, Braunschweig (in German). Publisher: Vieweg & Sohnn (1918)

English Translation: Forced oscillations with changing natural frequencies and their technical significance.

[3] Kurt Magnus: Vibrations, Blackie, London & Glasgow, 1965. Translated from German, lectures at Technische Hochschule Stuttgart.

In particular, Chap. 5.4.3 Harmonic excitation of damped nonlinear oscillators.

[4] Ali Hasan Nayfeh: Introduction to Perturbation Techniques, John Wiley & Sons New York NY, 1973. In particular, Chap. 4.5 Method of Multiple Scales.

[5] Ali Hasan Nayfeh and Dean T. Mook: Nonlinear Oscillations, John Wiley & Sons New York NY, 1979.

In particular, Chapter 4: Forced Oscillations of Systems Having a Single Degree of Freedom. The Preface lists a large number of text books spanning the years 1947 to 1978. The *Method of Multiple Scales* is introduced in Chap. 2.3.3, and used repeatedly. Sec. 4.1.1 *Primary resonanaces* uses multiple scales to explain the jump phenomenon.

[6] Peter Hagedorn: Non-linear Oscillations (Translated and edited by Wolfram Stadler), Clarendon Press, Oxford, 1981.

Chapter 1, The Mathematical Pendulum, quickly moves to a consideration of the Duffing resonator.

[7] Ivana Kovacic and Michael J. Brennan: The Duffing Equation - Nonlinear Oscillators and their Behaviour, John Wiley & Sons (2011).

[8] Hiroshi Yabuno: Free vibration of a Duffing oscillator with viscous damping, Chap. 3 in Ref.[7].

[9] Livija Cveticanin: Analysis Techniques for the Various Forms of the Duffing Equation, Chap. 4 in Ref.[7].

[10] Tamas Kalmar-Nagy and Balakumar Balachandran: Forced Harmonic Vibration of a Duffing Oscillator with Linear Viscous Damping, Chap. 5 in Ref.[7]. In particular section 5.3.1

[11] Asok Kumar Mallik: Forced Harmonic Vibration of a Duffing Oscillator with Different Damping Mechanisms, Chap. 6 in Ref.[7]. In particular section 6.4.1

[12] Richard H. Rand: Lecture Notes on Nonlinear Vibrations, Dept. Theoretical & Applied Mechanics, Cornell University Ithaca NY, 2015. In particular section 4: The Forced Duffing Oscillator.

https://ecommons.cornell.edu/items/ca4770bc-fad3-4600-80ea-4c806499f525

[13] Wojciech Wawrzynski: Duffing-type oscillator under harmonic excitation with a variable value of excitation amplitude and time dependent external disturbances. Scientific Reports Vol. 11, Article 2889 (2021).

[14] Wojciech Wawrzynski: "The origin point of the unstable solution area of a forced softening Duffing oscillator", Scientific Reports Vol. 12, Article number: 4518 (2022)

[15] M.J. Brennan, I. Kovacic et al: "On the jump-up and jump-down frequencies of the Duffing oscillator", Journal of Sound and Vibration **318** (2008) 1250–1261.

[16] Frank R. Groves Jr.: Numerical solution of nonlinear differential equations using computer algebra, Int. Jnl. of Computer Mathematics, Vol. 13, Issue 3-4 (1983).

[17] Jack K. Hale, Oscillations in Nonlinear Systems, McGraw-Hill, New York, 1963. Republished by Dover in 1992.

In particular, Chapter 6: Periodic Solutions of Equations in Standard Form - Critical Cases; and Chapter 7: Practical Methods of Computing a Periodic Solution and Examples.
Note, Hale has a strong interest in (and worked examples of) the Van der Pol equation.

[18] Minoru Urabe: Galerkin's procedure for nonlinear periodic systems, Archive for Rational Mechanics and Analysis, Vol.20 p. 120-152 (1965).

[19] Minoru Urabe and Allen Reiter: Numerical Computation of Nonlinear Forced Oscillations by Galerkin's Procedure, Jnl. of Mathematical Analysis and Applications, Vol. 14, p. 107-140 (1966).

[20] Minoru Urabe: Periodic Solutions of Differential Systems, Galerkin's Procedure and the Method of Averaging. Jnl. of Differential Equations, Vol.2, p. 265-280 (1966)

[21] Leonhard Euler: De novo genere oscillationum (On a new class of oscillations), Commentarii academiae scientiarum Petropolitanae **11**, 1750, pp. 128-14. Republished in Opera Omnia: Series 2, Volume 10, pp. 78 – 97.

Translated by Sylvio Bistafa (2021).

https://scholarlycommons.pacific.edu/euler-works/126/

[22] Keith Worden: On Jump Frequencies In The Response Of The Duffing Oscillator, Journal of Sound and Vibration, **198**(4), pp. 522-525. (1996).

[23] D.W. Jordan and P.Smith: Nonlinear Ordinary Differential Equations, Oxford Applied Mathematics and Computing Science Series, Clarendon Press Oxford, 1977.

See Chap. 5 Perturbation Methods, and Chap. 7 Driven Response. In particular, Chap. 5.4-5.7. and Chap. 7.2-7.3 relate to the driven response and jump phenomena of the Duffing oscillator (or "cubic pendulum"). Chap 7.7: Subharmonics of Duffing oscillator (drive at $\omega/3$ produces oscillations at ω due to cubic term).

[24] Roger Poirier: Perpendicular Biased Ferrite-Tuned Cavities, Proc. 1993 Particle Accelerator Conf., Washington DC May 1993, pp. 753-757.

[25] Carl Friedrichs & G. Hulsey: The Effects of Temperature and RF Power Level on the Tuning of the Water-Cooled SSC Low-Energy Booster Cavity, Proc. 1993 Particle Accelerator Conf., pp. 803-805.

[26] Vladen E. Shapiro: Magnetic Losses and Instabilities In Ferrite Garnet Tuned RF Cavities For Synchrotrons, Journal of Particle Accelerators, 1994, Vol. 44(1), pp. 43-63.

[27] M. Parise: Prediction of the Lorentz Force Detuning and pressure sensitivity for a Pillbox cavity, Journal of Instrumentation Vol. 13 Technical Report T05010 (2018)

Nice concrete example of a geometry that is both useful and easy to analyze.

`https://doi.org/10.1088/1748-0221/13/05/T05010`

[28] Dietrich Schulze: "Ponderomotive Stability of RF Resonators and Resonator Control Systems", KFK-1493 Karlsruhe, Germany, 1971. Translation by Argonne National Laboratory ANL-TRANS-944.

[29] Lawrence R. Doolittle: Tuners, Microphonics, and Control Systems in Superconducting Accelerating Structures, Proc. Fourth Workshop on RF Superconductivity, KEK, Tsukuba, Japan, 1989, pp. 341-350.

[30] Vladimir Igorevich Arnold: Ordinary Differential Equations, translated by R.A. Silverman, The MIT Press, 1973.

In particular, Chapter 3 Linear Systems.

[31] C. G. J. Jacobi: De determinantibus functionalibus, J. reine angew. math., 22 (1841), p. 319–352. Gesammelte Werke 3, Georg Reimer, Berlin, 1884, 395–438.

[32] Haïm Brezis, Jean Mawhin, Petru Mironescu: A brief history of the Jacobian, HAL Id: hal-04059234 (2023).

HAL is a multidisciplinary open archive for freely sharing published and unpublished research results. In France, HAL is the national archive chosen by the French scientific and academic community for the open dissemination of its research results.